WorldView-3 satellite maps methane plumes at very high spatial resolution

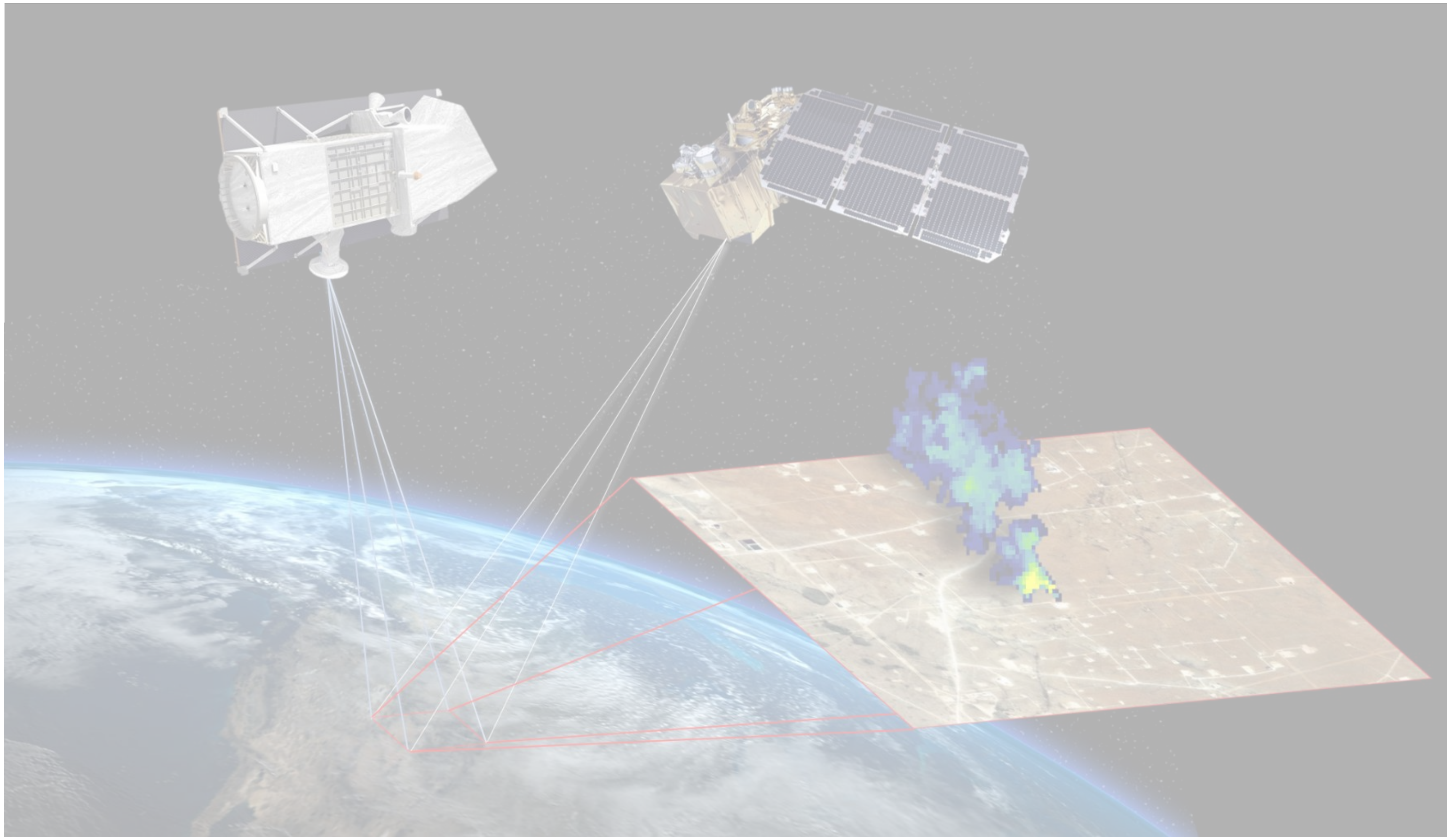

Elena Sánchez-García[1], Javier Gorroño[1], Itziar Irakulis-Loitxate[1], Daniel Varon[2], Luis Guanter[1]

[1]Universitat Politècnica de València, [2]Harvard University

Table of contents

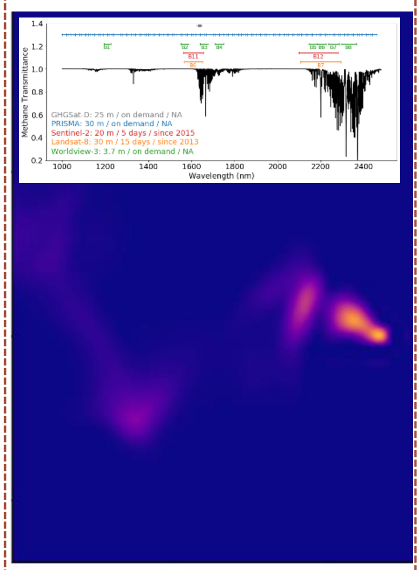

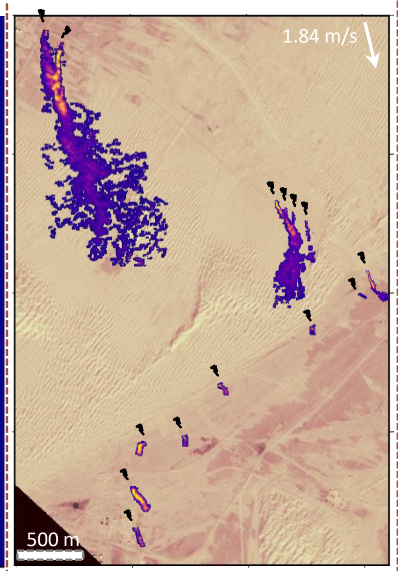

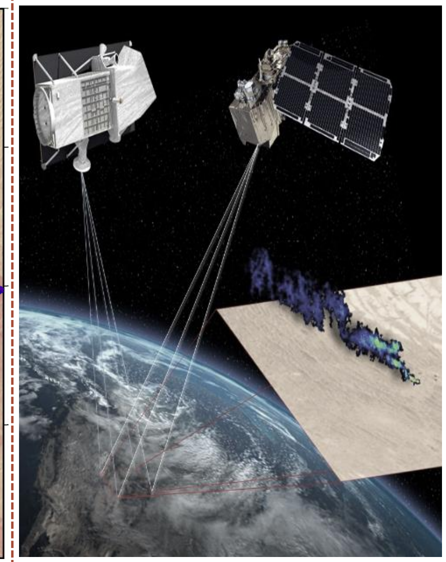

Sánchez-García et al. (in review at AMT)
https://doi.org/10.5194/amt-2021-238

Table of contents

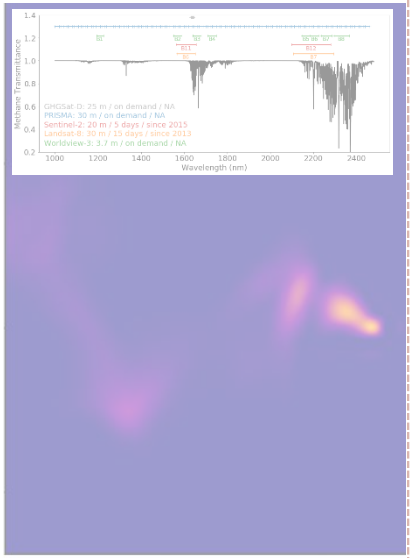

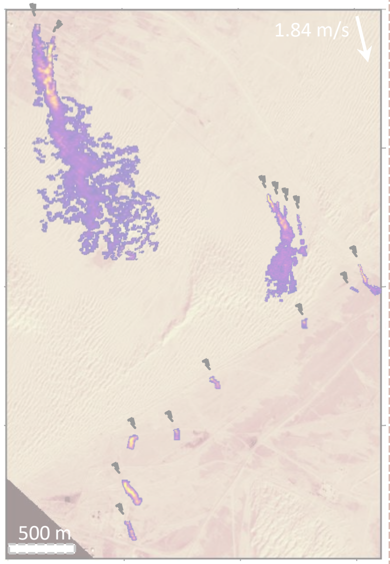

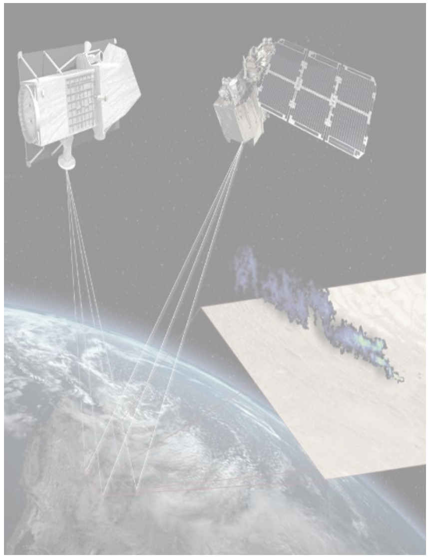

Methane

√ Substantial advances towards the **detection and quantification of methane point emissions from space**.

√ Up to date:

Can focus on the detection of **single emitters**

GHGSat: optimized for the monitoring of methane point emissions → Varon et al. (2019, 2020).

Hyperspectral imagers covering 400-2500 nm (ZY1 AHSI, GF5 AHSI, & PRISMA) → Irakulis-Loitxate et al. (2021a; 2021b) and Guanter et al. (2021).

- High sensitivity.
- Spatial sampling (25-50 m).
- … but acquisitions sparse in time and space.

Multispectral missions (S2, Landsat-7 & L8) originally developed for land applications spatial and temporal resolution (20-30 m, & 5-15 days) , can help to overcome this limitation with frequent and spatially-continuous observations (Varon et al., 2021), albeit with a substantially lower sensitivity to methane.

Methane

√ Substantial advances towards the **detection and quantification of methane point emissions from space**.

√ Up to date:

Can focus on the detection of **single emitters**

GHGSat: optimized for the monitoring of methane point emissions → Varon et al. (2019, 2020).

Hyperspectral imagers covering 400-2500 nm (ZY1 AHSI, GF5 AHSI, & PRISMA) → Irakulis-Loitxate et al. (2021a; 2021b) and Guanter et al. (2021).

- High sensitivity.
- Spatial sampling (25-50 m).
- … but acquisitions sparse in time and space.

Multispectral missions (S2, Landsat-7 & L8) originally developed for land applications spatial and temporal resolution (20-30 m, & 5-15 days) , can help to overcome this limitation with frequent and spatially-continuous observations (Varon et al., 2021), albeit with a substantially lower sensitivity to methane.

Identify **regions** of strong concentrations

Methane mapping efforts with all those missions greatly benefit from the synergistic use of **TROPOMI** → Lauvaux et al., 2021.

…drawback ?

Methane

… new breakthrough of emission detection thresholds using **VHR SWIR** measurements from **WorldView-3** satellite. Until now, only possible for airborne instruments, like AVIRIS & AVIRIS-NG spectrometers operated by NASA JPL.

→ Accurate **identification of the particular infrastructure elements responsible for the emissions** and more precise quantification of emission rates (spatial resolution of 3.7 m).

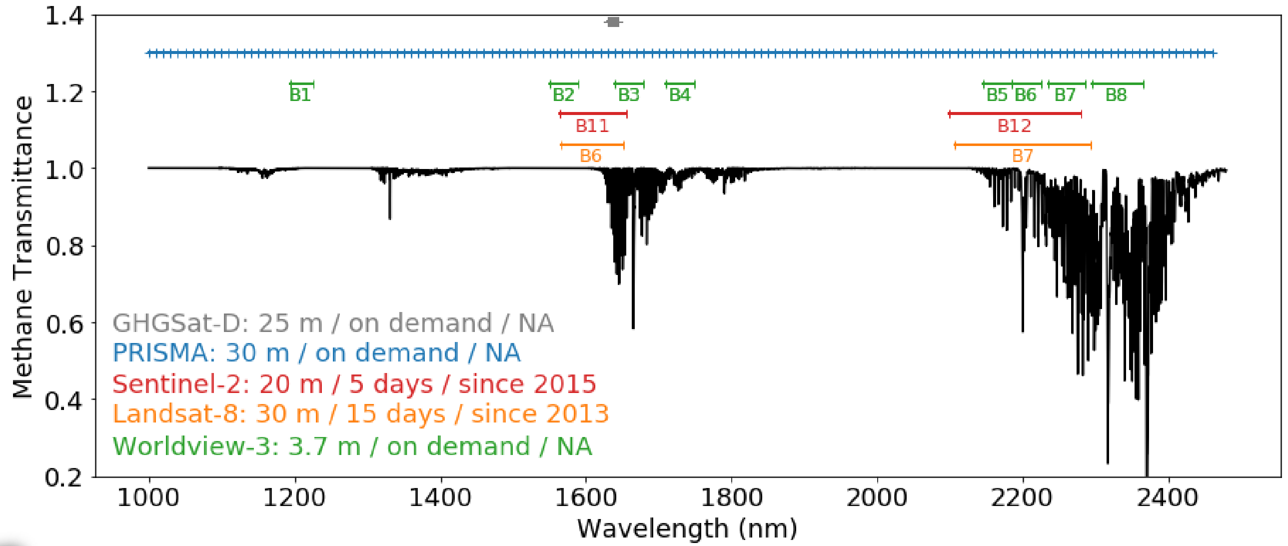

WV-3: High spatial resolution, high SNR and rich spectral coverage of the strong methane absorption feature ~2300 nm. Furthermore, **pointing capabilities** able to deliver a daily revisit or better over critical infrastructure.

Unique features to fill an important observational gap in international satellite methane monitoring capabilities.

INTRODUCTION

Aims of the work

√ We report on the great **potential of** the WorldView-3 (**WV-3**) satellite mission **for methane mapping**

Working objectives

- Propose a retrieval methodology based on the calculation of methane concentration enhancements from pixel-wise estimates of methane transmittance at WV-3 SWIR band 7 (2235-2285 nm), which is positioned at a highly-sensitive methane absorption region.

- Carry out a sensitivity analysis based on end-to-end simulations to understand retrieval errors and detection limits.

- Show through the simulated results the good performance of WV-3 for methane mapping, especially over bright and homogeneous areas.

- Positive plume detections obtained from the study sites: O&G extraction fields in Algeria and Turkmenistan, and the Shanxi coal mining region in China.

Table of contents

Methane retrieval

√ Estimate **methane concentration enhancement:**

→ for *hyperspectral*, by fitting highly-resolved obsv in the SWIR spectral region to a modelled radiance spectrum.

→ for *multispectral*, from **increases in <u>methane transmittance</u>** within the image.

1. Normalize the radiance affected by methane absorption by a “methane-free” reference band.

In the absence of multi-temporal data, this reference can be built from one or several neighboring channels mostly “methane-free”.

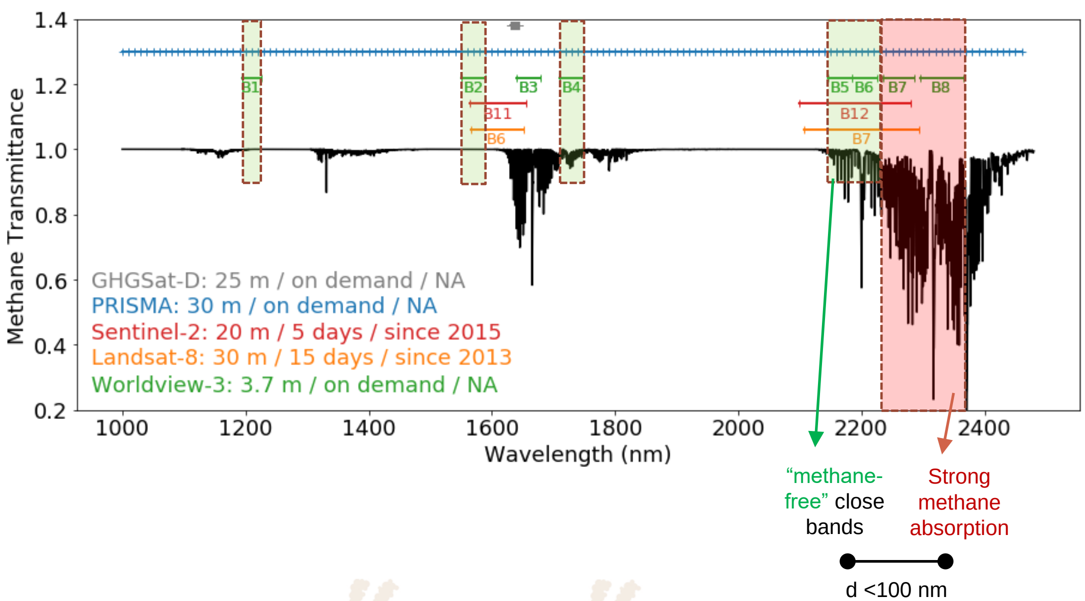

The **plume transmittance** T_{plume} can be described as:

$$\boxed{T_{plume}(\lambda) \sim \frac{L}{L_{ref}} = e^{-AMF \,.\, \sigma_{CH_4} \,.\, \Delta XCH_4}}$$

where:

L = radiance of the methane-sensitive band
L_{ref} = radiance of the “methane-free” reference band
AMF = air mass factor,
σ_{CH_4} (ppm^{-1}) = methane absorption cross section
ΔXCH_4 (ppm) = methane concentration enhancement (increment produced by the plume from the background).

METHODS

Methane retrieval

√ Estimate **methane concentration enhancement:**

→ for *hyperspectral*, by fitting highly-resolved obsv in the SWIR spectral region to a modelled radiance spectrum.

→ for *multispectral*, from **increases in <u>methane transmittance</u>** within the image.

1. Normalize the radiance affected by methane absorption by a "methane-free" reference band.

In the absence of multi-temporal data, this reference can be built from one or several neighboring channels mostly "methane-free".

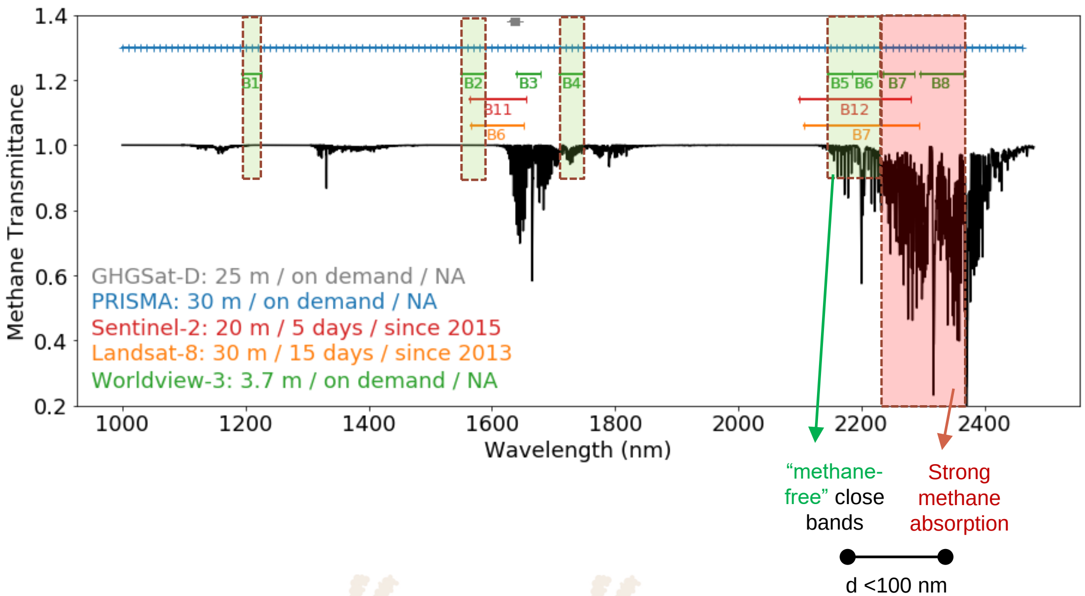

The **approach** to obtain the **Lref** :

- Simplest form: $\frac{B7}{B5}$, bands spectrally close and correlated.
- Proposal: $\frac{B7}{B7MLR}$, MLR of B1-B6 with B7 as target band.

Note:

Despite B8 being more sensitive to methane absorption, it has shown lower spectral correlation with B1-B6 bands as compared to B7.

B3 & B6 marginally sensitive to methane; so: B3 is excluded but B6 remains due to is closeness to B7.

METHODS

Methane retrieval

√ Estimate **methane concentration enhancement:**

→ for *hyperspectral*, by fitting highly-resolved obsv in the SWIR spectral region to a modelled radiance spectrum.

→ for *multispectral*, from **increases in methane transmittance** within the image.

1. Normalize the radiance affected by methane absorption by a "methane-free" reference band.

2. Methane plume quantification by isolating ΔXCH_4 in: $\boldsymbol{T_{plume}}(\lambda) \sim \frac{\boldsymbol{L}}{\boldsymbol{L_{ref}}} = e^{-AMF \,.\, \sigma_{CH_4} \,.\, \Delta XCH_4}$

$$\boxed{\Delta XCH_4 = \frac{-\,log(\mathbf{L}/\mathbf{L_{ref}})}{\mathrm{AMF}\,\cdot\,\sigma_{CH_4}}}$$

- Then, ΔXCH_4 becomes a function of the AMF and the radiance ratio L/L_{ref} of SWIR B7 (2235-2285 nm).

- A Look-Up Table is generated so that the relationship between these two quantities and the ΔXCH_4 is established →

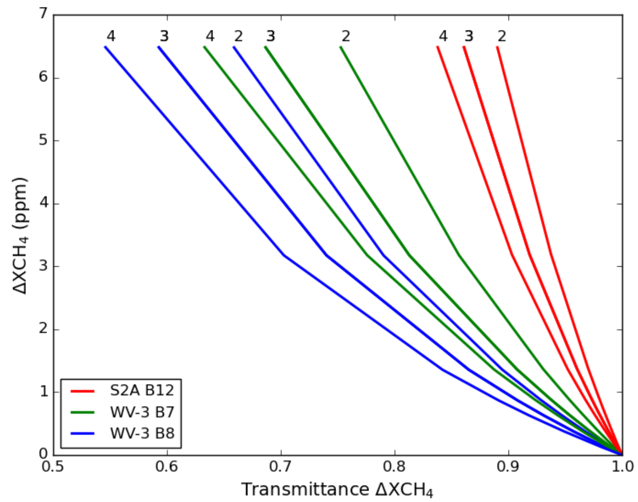

LUT relationship between $\boldsymbol{T_{plume}}$ & ΔXCH_4 for the methane absorption bands (~2300 nm) of S2A, WV-3 B7 and WV-3 B8.

Curves given for 3 different AMF values representing angular conditions for both SZA and VZA: 0,0; 60,0 and 60,60 (labels 2 to 4).

METHODS

Detection of methane plumes

1º. Visual inspection of the retrieved ΔXCH_4 maps ➔ distinguish plume characteristic shape from background.

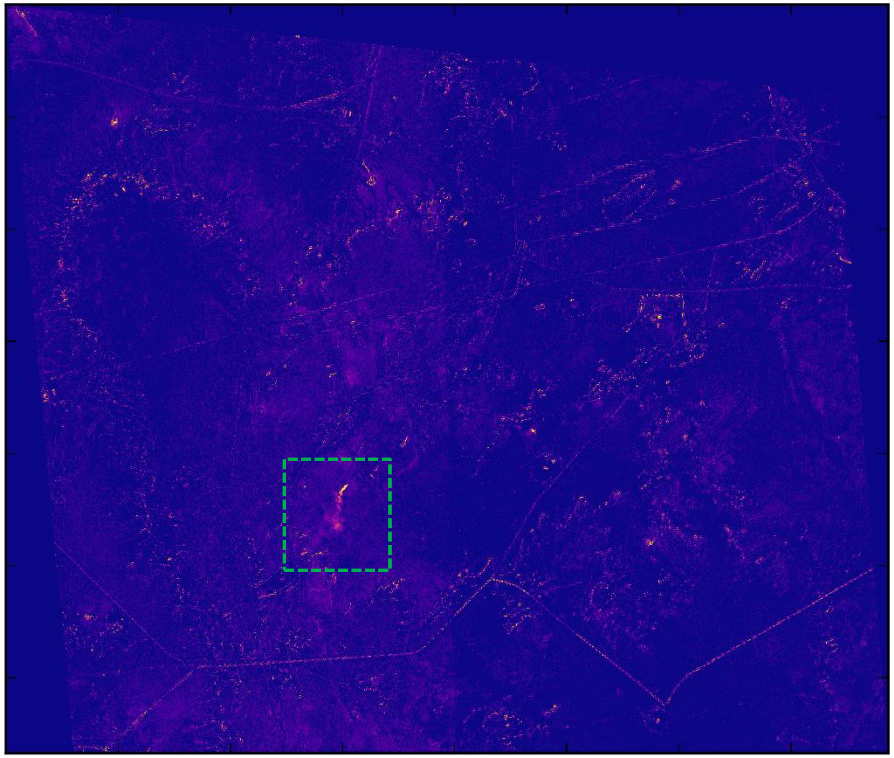

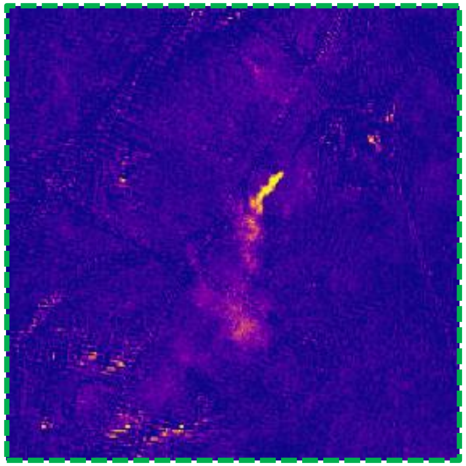

Detection of methane plumes

1º. Visual inspection of the retrieved ΔXCH4 maps ➔ distinguish plume characteristic shape from background.

2º. Consistency with GEOS-FP **wind speed & direction data** ➔ gas plume origin at high ΔXCH_4 values & decrease progressively downwind.

3º. Collocate with high spatial resolution true color images (Google Earth & B1 WV-3) to **identify the underlying infrastructure** responsible for the emission.

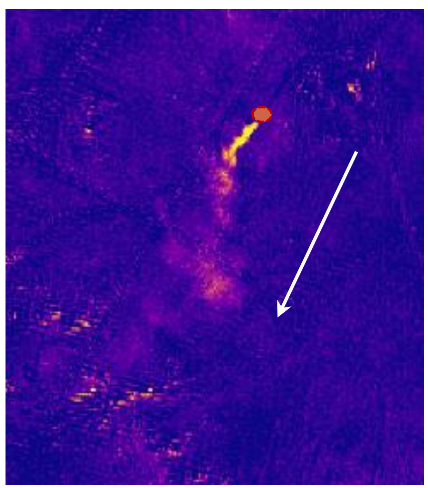

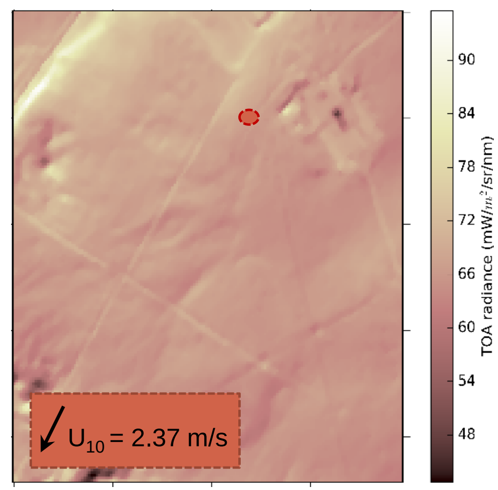

Detection of methane plumes

4º. Zooms in on each real plume to isolate it from the background & **compute the total area covered by the emission** ➔ semi-automatic process**:**

- **Mask** at the 95% confidence level and a square dilation mask of several pixels.
- Finally, the **detected outliers** in the vicinity of the plumes are removed through feature recognition.

Example:

ΔXCH4 map

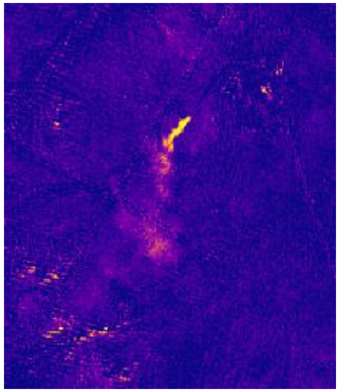

σ+dilate+outliersDetection -> Mask

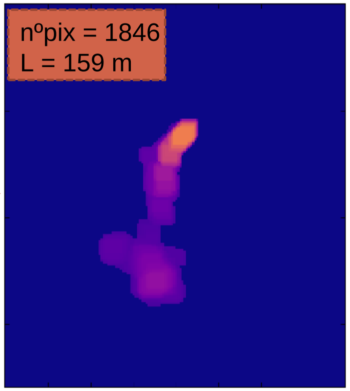

cleaned ΔXCH4 map

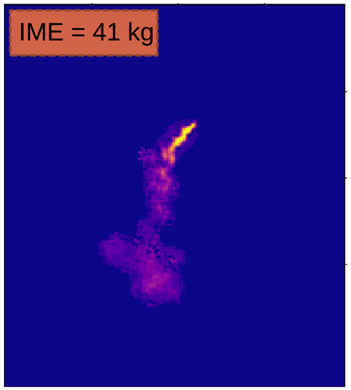

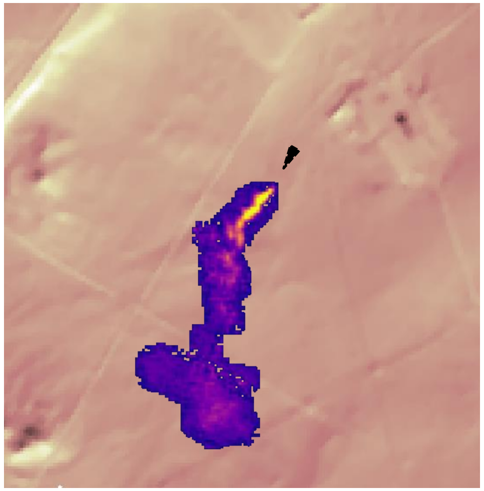

METHODS

Estimating emission flux rates

√ Once the plumes are correctly defined, the **associated flux rate Q** is obtained **by applying the so-called IME model**
~ measure of the total excess mass of observed methane.

1º. ΔXCH_4 values (ppm) ➔ (Kg)

2º. Compute IME in kg for each plume as the total sum of the ΔXCH4 pixels enclosed by the plume mask.

3º. Relate the **Q** emission flux rate **with** the calculated **IME** & obtain its associated uncertainty based on a Monte Carlo propagation:

$$\boxed{\boldsymbol{Q}\left(\frac{\boldsymbol{kg}}{\boldsymbol{h}}\right) = \frac{U_{eff}\left(\frac{\mathrm{m}}{\mathrm{s}}\right)\cdot \mathrm{IME\ (kg)} \cdot 3600}{\mathrm{L\ (m)}}}$$

$$\begin{cases} \text{if L} < 200\ \text{m} \rightarrow U_{eff}\left(\frac{m}{s}\right) = 0.12 \cdot U_{10} + 0.38 \\ \text{if L} > 200\ \text{m} \rightarrow U_{eff}\left(\frac{m}{s}\right) = 0.34 \cdot U_{10} + 0.44 \end{cases}$$

U_{eff} = effective wind speed derived from WRF-LES according to Varon et al. (2018) methodology & tuned at ~4 m WV-3 resolution and 1-sigma white noise (120 to 370 ppb depending on the site).

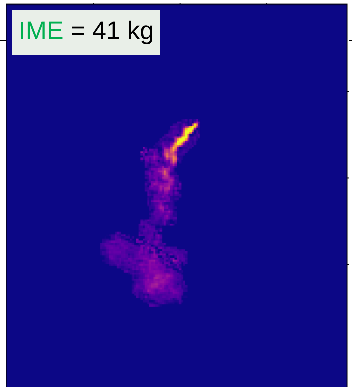

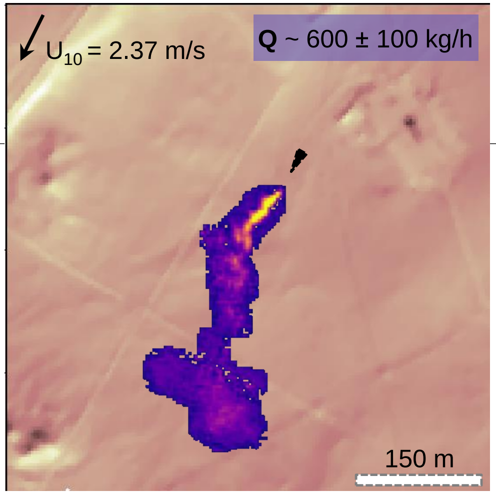

Sensitivity analysis based on end-to-end simulations

√ **Simulation generated by convolving WV-3 TOA radiance** scenes **with synthetic methane plumes** generated with the WRF-LES. Effects such as instrument noise or angular pixel dependencies from the real scenes are also in the resulting simulations.

End-to-end simulations for three **different** sites whose spectral response behave differently regarding their **surface conditions**:

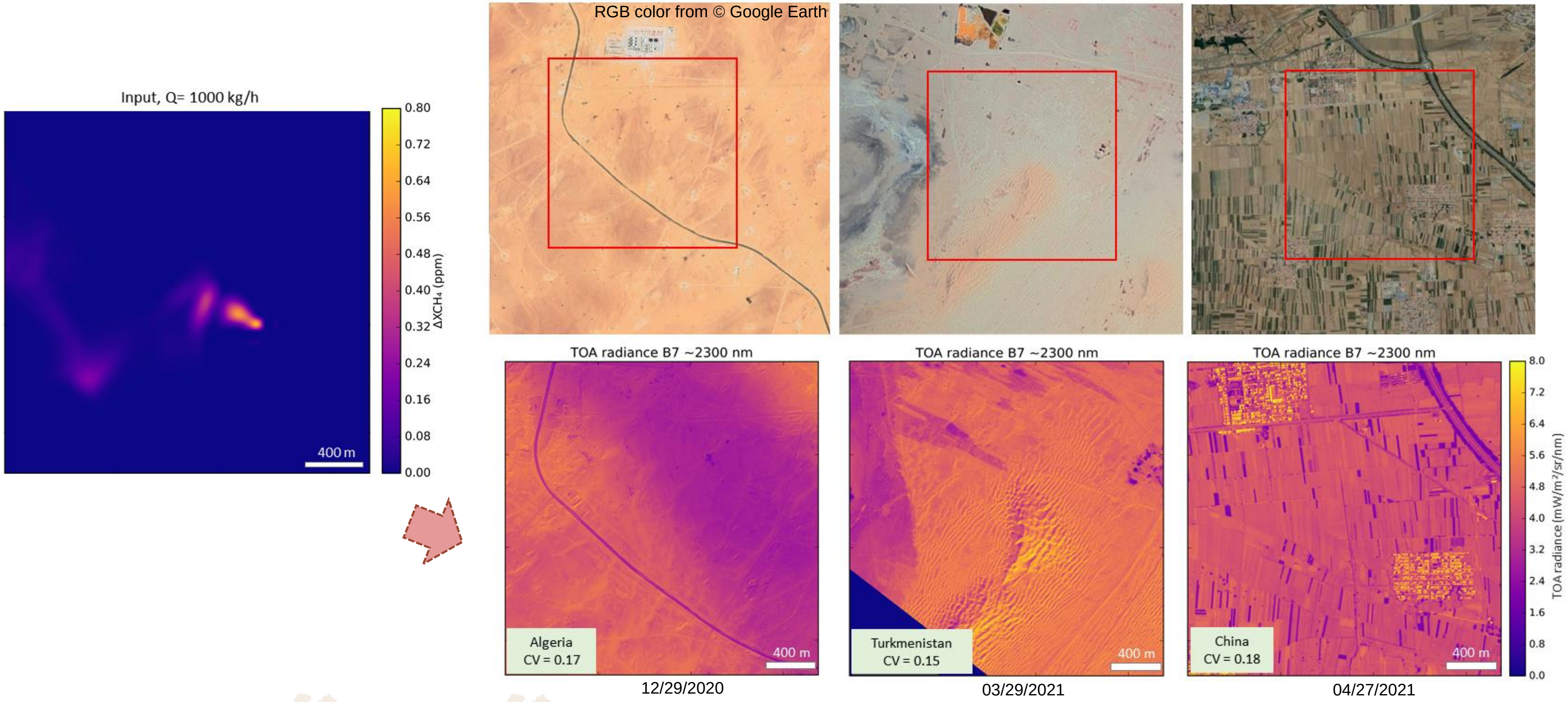

Table of contents

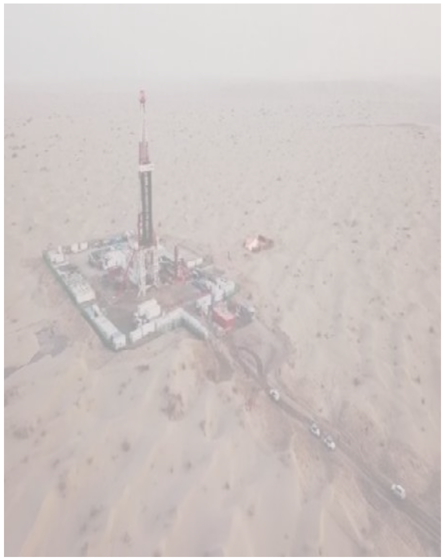

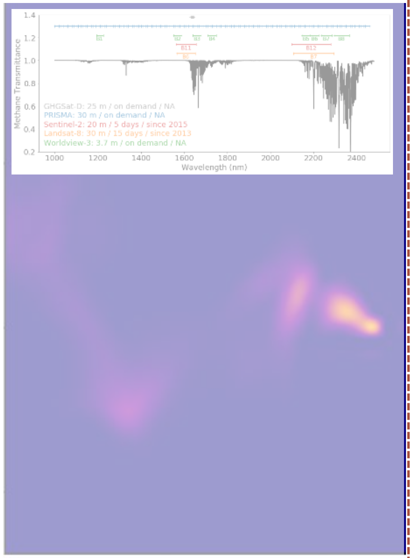

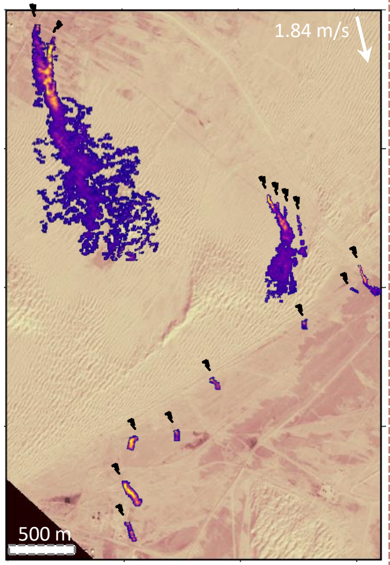

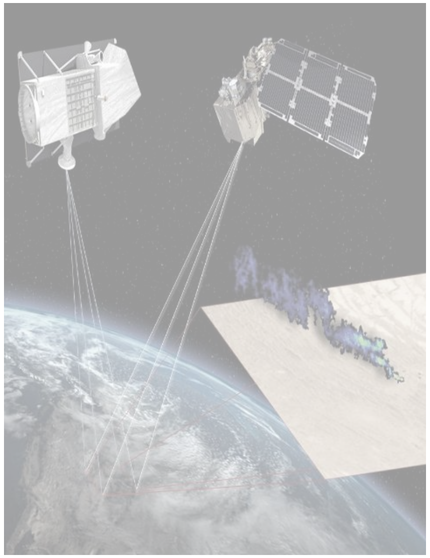

Retrieval performance with simulated plumes

√ **Best approach to calculate a "methane-free" reference band?** ⟶ resulting ΔXCH_4 maps

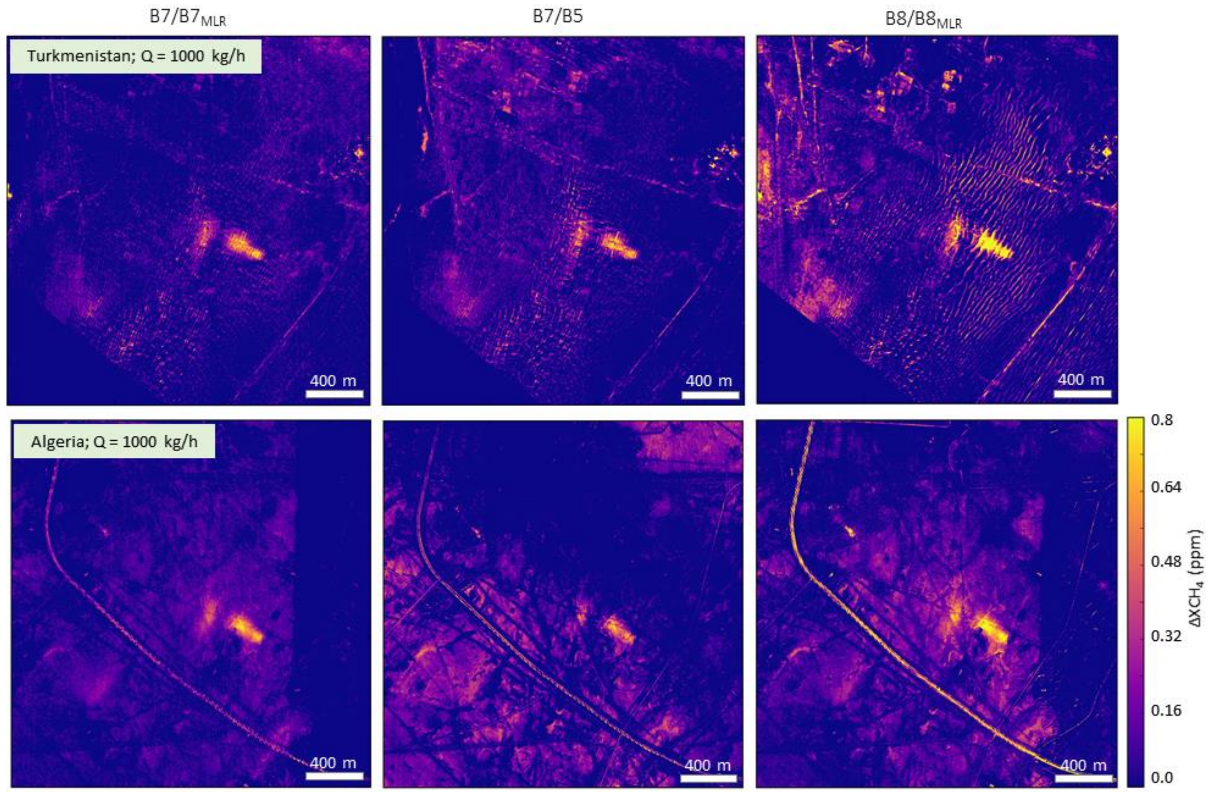

Retrieval performance with simulated plumes

√ **Best approach to calculate a "methane-free" reference band?** → resulting ΔXCH_4 maps

Best compromise between detection sensitivity and low outlier generation (clear shape of the plume).

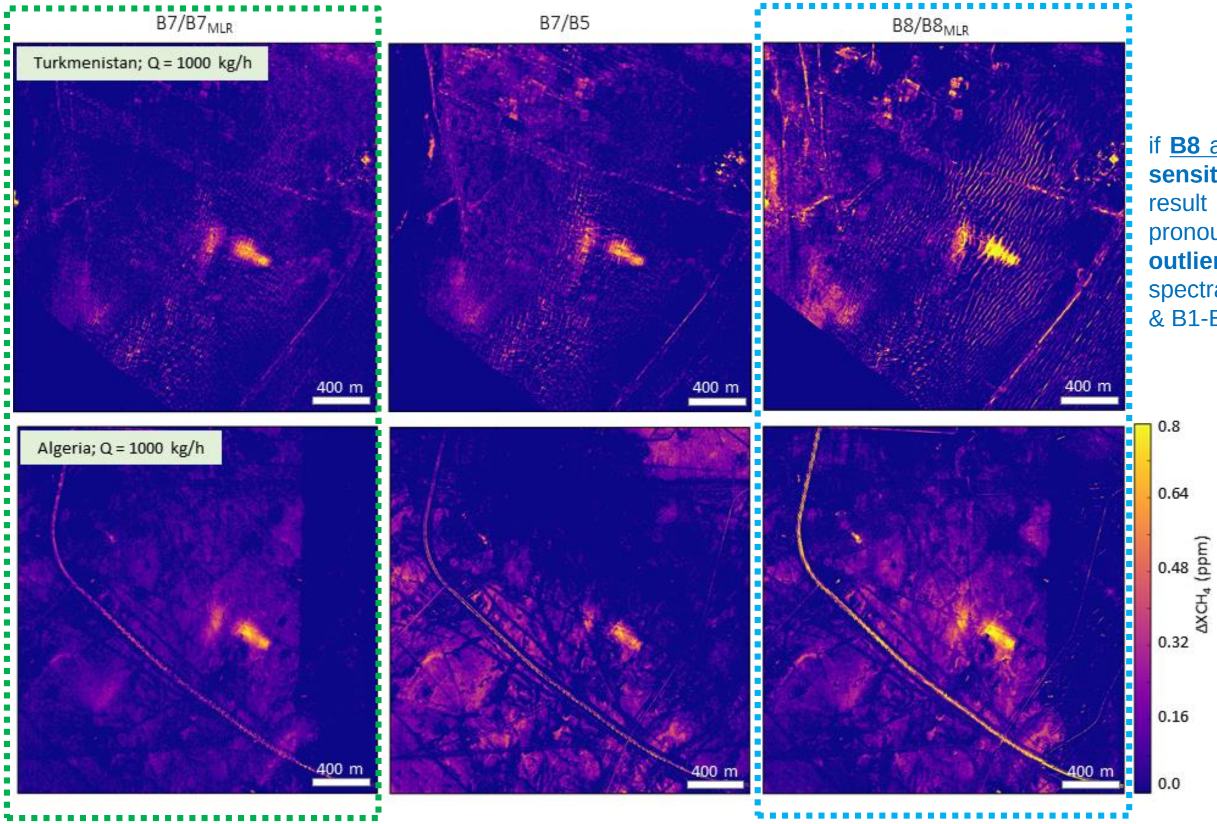

if B8 as target -> **largest sensitivity**. However, the result also exhibits a pronounced impact of **outliers** due to the larger spectral distance from B8 & B1-B6.

Retrieval performance with simulated plumes

√ retrieval **detection limit?** ⟶ ΔXCH_4 maps obtained with the selected methodology:

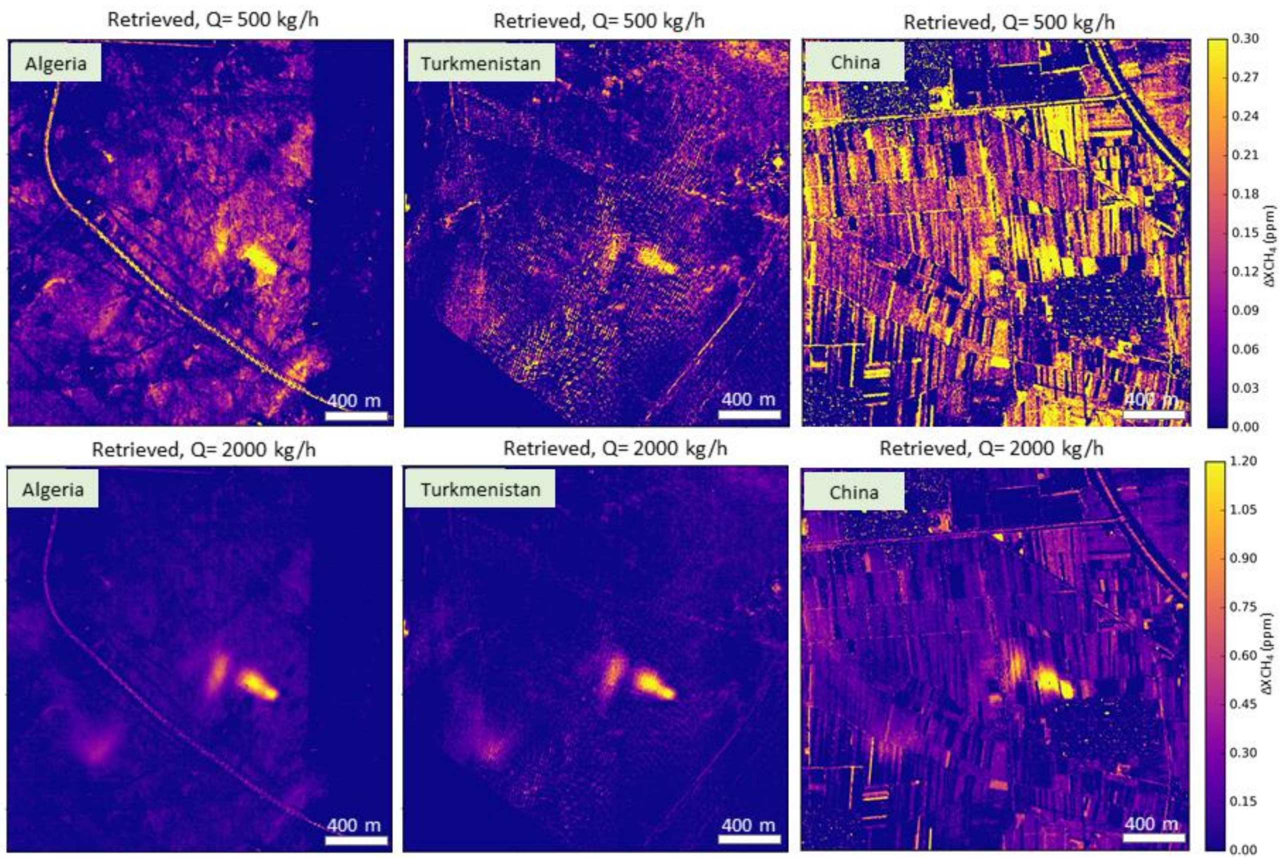

As expected, best results in Turkmenistan & Algeria.

- The **Algeria** maps show a discontinuity on the right side of the image.
- The **China** map presents many features that alter the retrieval and require higher methane plume signals in order to positively detect them.

RESULTS

Retrieval performance with simulated plumes

√ retrieval **detection limit?** → ΔXCH_4 maps obtained with the selected methodology:

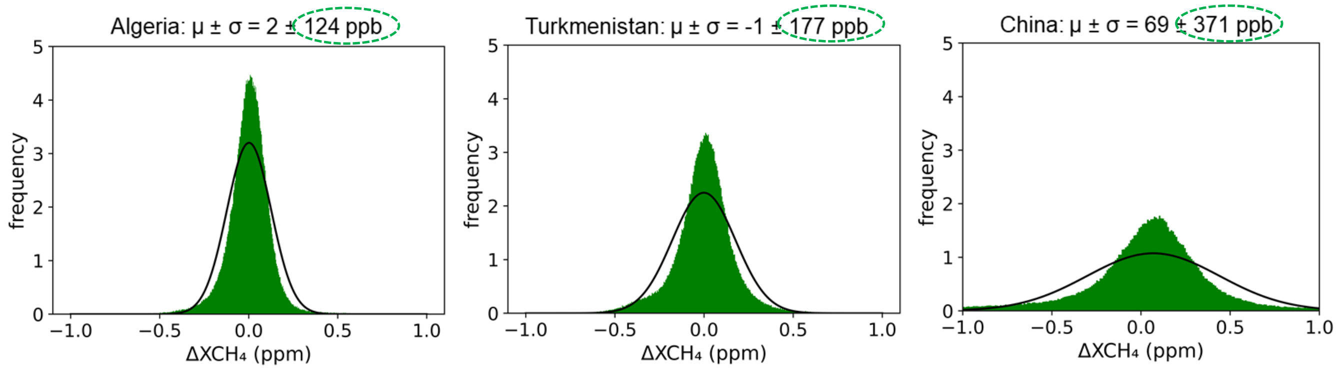

Distribution of the retrieved ΔXCH_4 maps

- 1-sigma retrieval errors sensibly larger than hyperspectral missions due to the increased surface variability.
- Non-normal behavior already present in the radiance ratio $L/L_{ref.}$

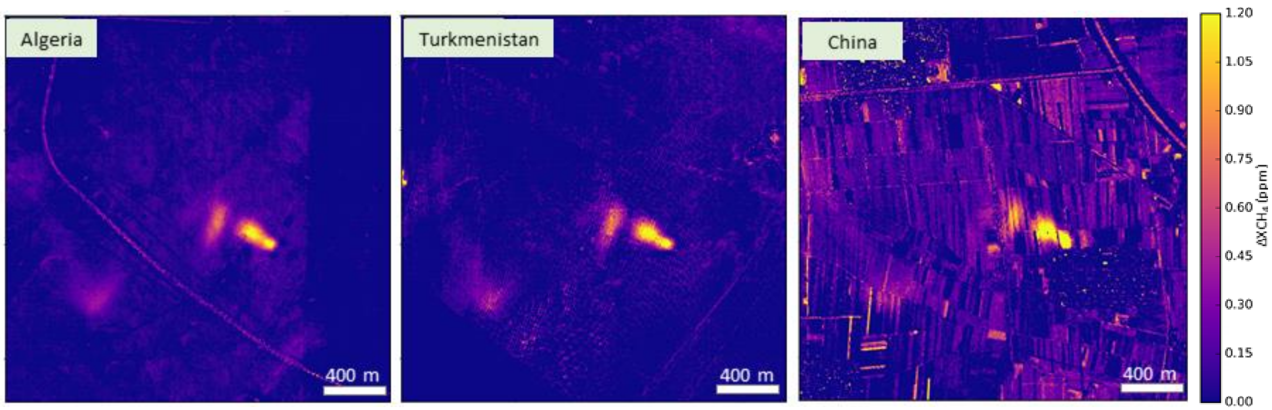

Methane plumes isolated from the background considering the noise levels & the explained procedure.

Retrieval performance with simulated plumes

√ Test of methane detection limits.

Figure displays the **relationship** between **retrieved IME &** known **reference input** values for the simulations at the 3 sites.

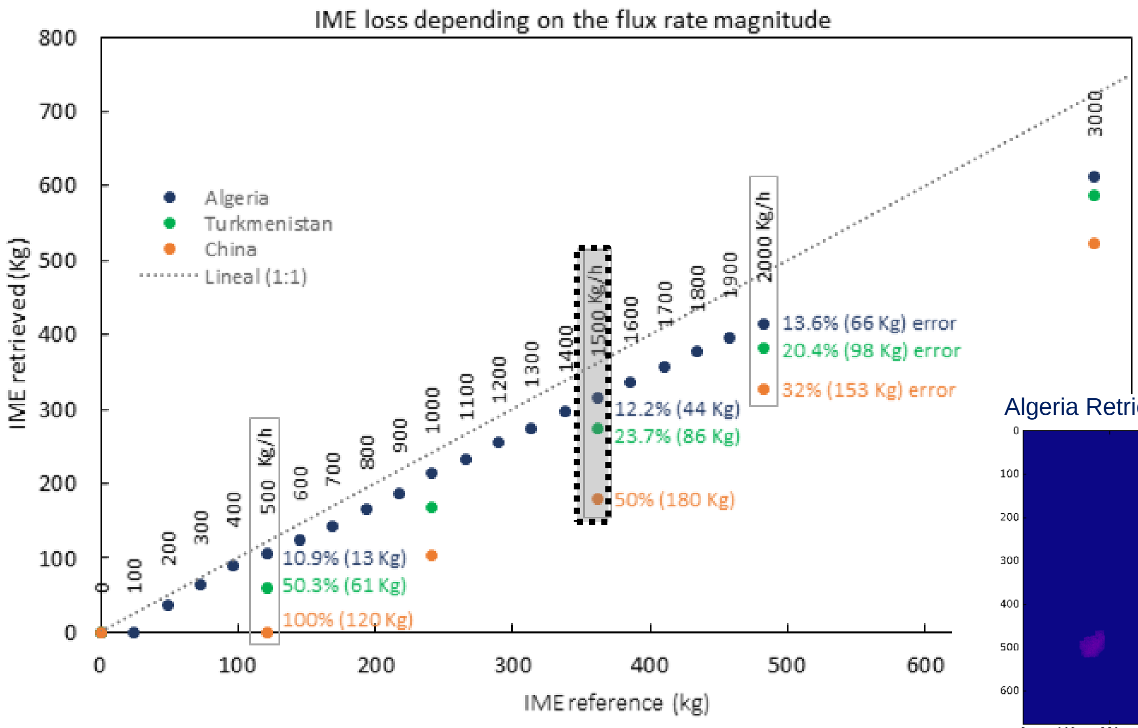

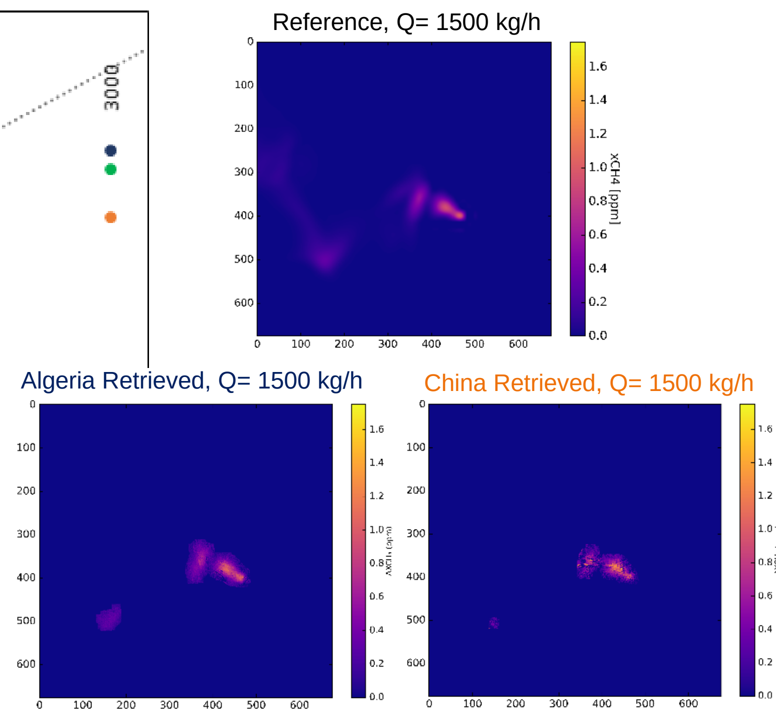

Retrieval performance with simulated plumes

√ **Test of methane detection limits.**

Figure displays the **relationship** between **retrieved IME &** known **reference input** values for the simulations at the 3 sites.

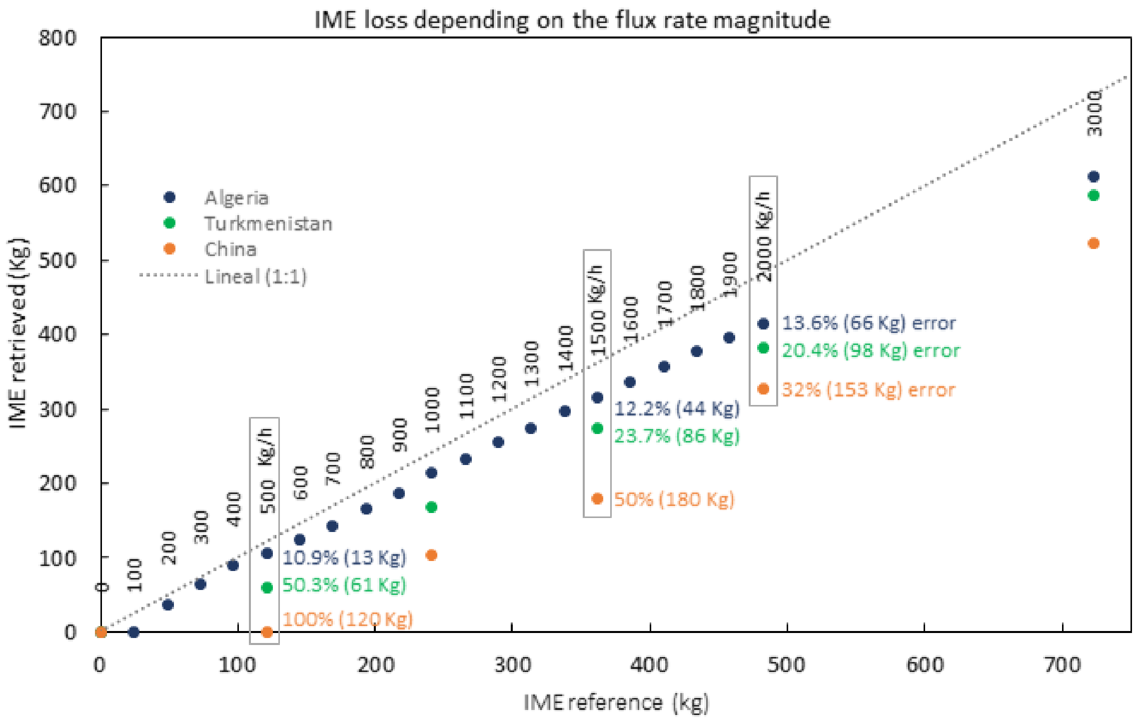

- The results highlight a **general underestimation** of the retrieved IME values.
- The missing fractions of the total IME are larger for China & lowest for Algeria.
- This reinforce the importance of surface heterogeneity on the performance retrieval.

Real case studies of methane detection

√ We work with **7 SWIR WV-3 images** covering four different areas (known regional methane hotspots).

√ Precise locations of **26 different point source emissions** over the 275 km^2 analyzed:

Site	Emitter location	Date	nºpix	L (m)	u_{10} (m/s)	u_{eff} (m/s)	IME (kg)	Q (kg/h)
Hassi Messaoud Oil field (Algeria)	Pipeline (31.778ºN, 5.995ºE)	2020/12/29	3363	215	6.14	2.53	74	3100 ± 1300
	Pipeline (31.768ºN, 6.000ºE)		3155	208			57	2500 ± 1000
	Pipeline (31.797°N, 6.011°E)		924	112		1.12	13	500 ± 200
	Pipeline (31.742ºN, 5.895ºE)	2021/01/17	1846	159	2.37	0.66	41	600 ± 100
Korpezhe O&G field (Turkmenistan South)	Ground Flare (38.494ºN, 54.198ºE)	2021/03/29	16956	482	3.93	1.78	1353	13000 ± 4800*
	Ground Flare (38.557ºN, 54.200ºE)		13188	425			287	3100 ± 1100*
Goturdepe field (Turkmenistan North); Eastern image	Pipeline (39.474ºN, 53.743ºE)	2021/04/10	20786	533	9.63	3.71	1390	35000 ± 15000
	Pipeline (39.462ºN, 53.775ºE)		7424	319			118	5000 ± 2200
Goturdepe field (Turkmenistan North); Western image	Two-point emitters (39.498ºN, 53.636ºE & 39.497ºN 53.638ºE)	2021/03/29	44689	782	1.84	1.07	496	2400 ± 700
	Four plumes around (39.485°N, 53.663°E)		8900	349			105	1200 ± 300
	Pipeline (39.480°N, 53.671°E)		3957	233			11	200 ± 60
	Two small plumes around (39.480°N, 53.671°E)		185	50		0.6	0.8	30 ± 10
			198	52			0.9	40 ± 20
	Five smaller southern plumes around (39.469°N, 53.649°E)		116	40			3	200 ± 30
			105	38			3	200 ± 30
			537	86			14	400 ± 70
			1842	159			61	800 ± 200
			1020	118			27	500 ± 90
Coal mines in Shanxi (China)	Xiligaocun (36.257°N, 112.923°E)	2021/04/27	6470	298	5.89	1.09	129	3800 ± 1600
	Wangzhuang Beili two-point emitters (36.247°N, 112.989°E & 36.246°N, 112.989°E).		7042	310			126	3600 ± 1500
	Taoyuancun (36.234°N, 112.946°E)		1278	132		2.44	24	700 ± 200

Real case studies of methane detection

√ The **uncertainties** obtained **for the different flux rates**, cover a **range of 15 to 45%**, being dominant the U_{10} uncertainty source

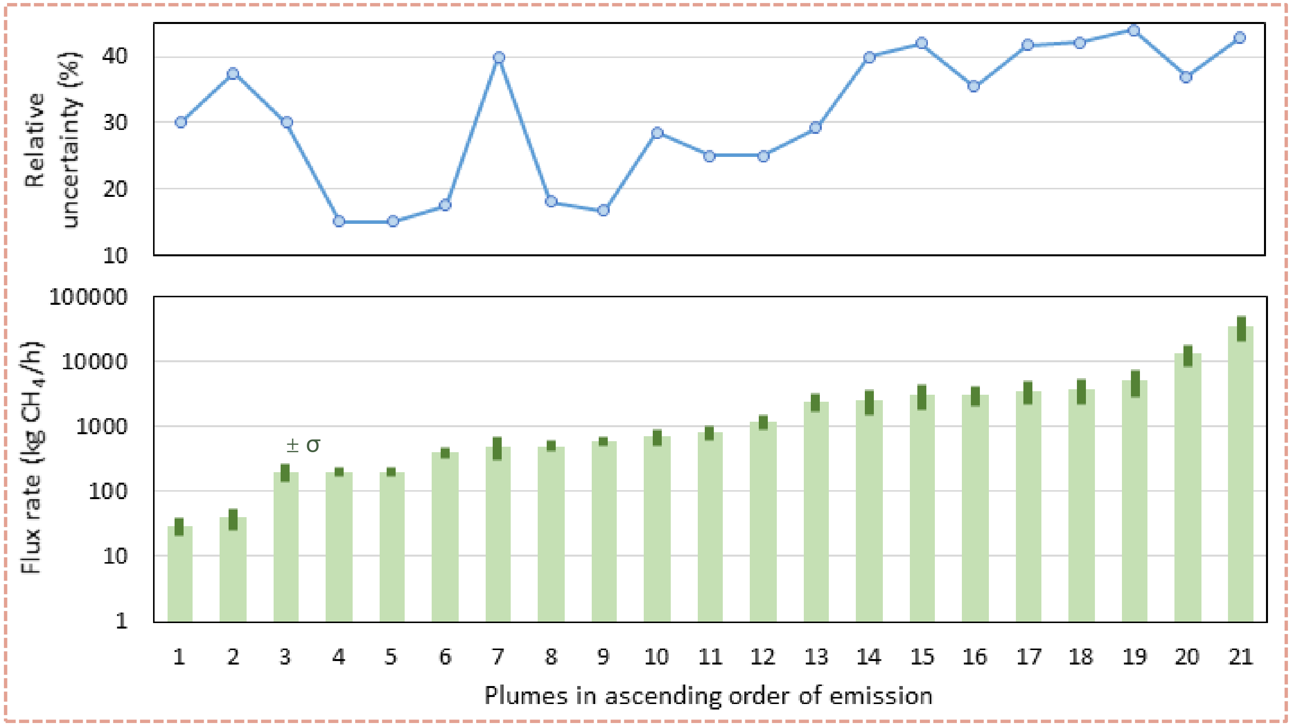

Correlation of Q uncertainty (± σ) with:

- 0.45 with the Q level.
- 0.15 with the IME value.
- 0.85 with $\mathbf{U_{eff}}$.

Real case studies of methane detection

Angular configuration scheme

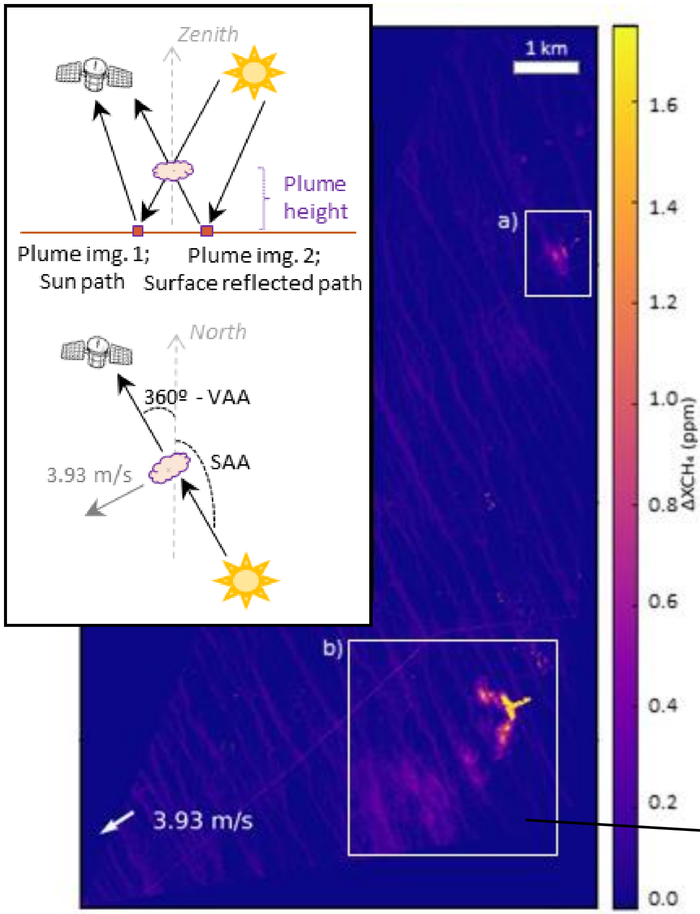

√ **Importance of geometric considerations for high-spatial methane quantification**:

- ΔXCH_4 map from Turkmenistan South on 29th March 2021 showing **two plumes with a particular shape, dual-plume structure,** as a consequence of the orthogonal alignment of the sun-to-satellite plane with respect to the wind direction → 1/2 plume mask to Q estimate.
- Despite the geometric and soil morphology effects (NW-SE noise pattern), both **emission sources** are easily **distinguished by the high ΔXCH_4 values** & the unmistakable **diffuse shape** of the **tail downwind**.

This massive southern plume extends up to 3 km, but our retrieved mask to calculate Q only takes the most integral part...

Real case studies of methane detection

√ **O&G ground flare emitters** often used in the burning of gaseous waste (already reported by Irakulis-Loitxate et al. 2021):

b) panel → Plume emerging from a gas pipeline near the compressor station. Despite the first announcement in Varon et al. (2019) and subsequent shutdown of the leak, this emitter source is once again spreading methane.

a) panel → Plume with a flux rate four times smaller.

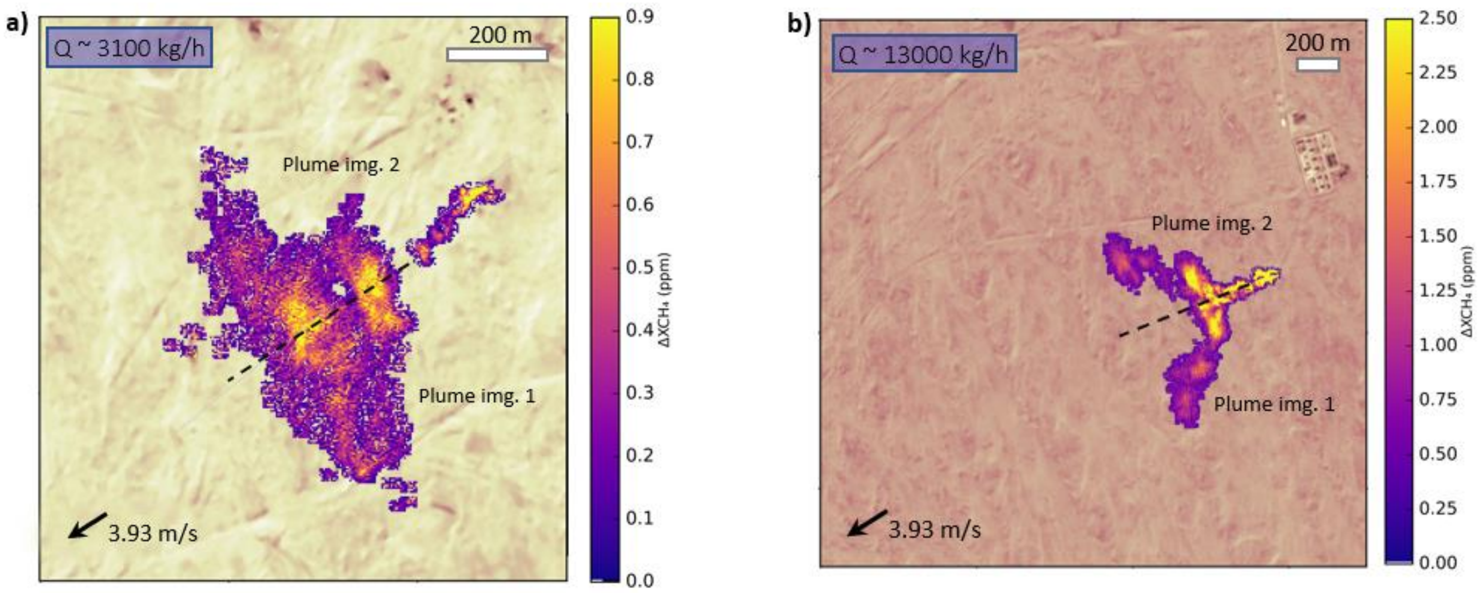

Real case studies of methane detection

√ **The area with the largest number of emitters** corresponds to the **Goturdepe O&G field** in North Turkmenistan.

A total of 16 different plumes are detected throughout this basin, one of the oldest oil piping systems.

Eastern image on 10th April 2021:

Two elongated plumes (consequence of strong wind). Originate from two-point sources registered also in Irakulis-Loitxate et al. (2021b).

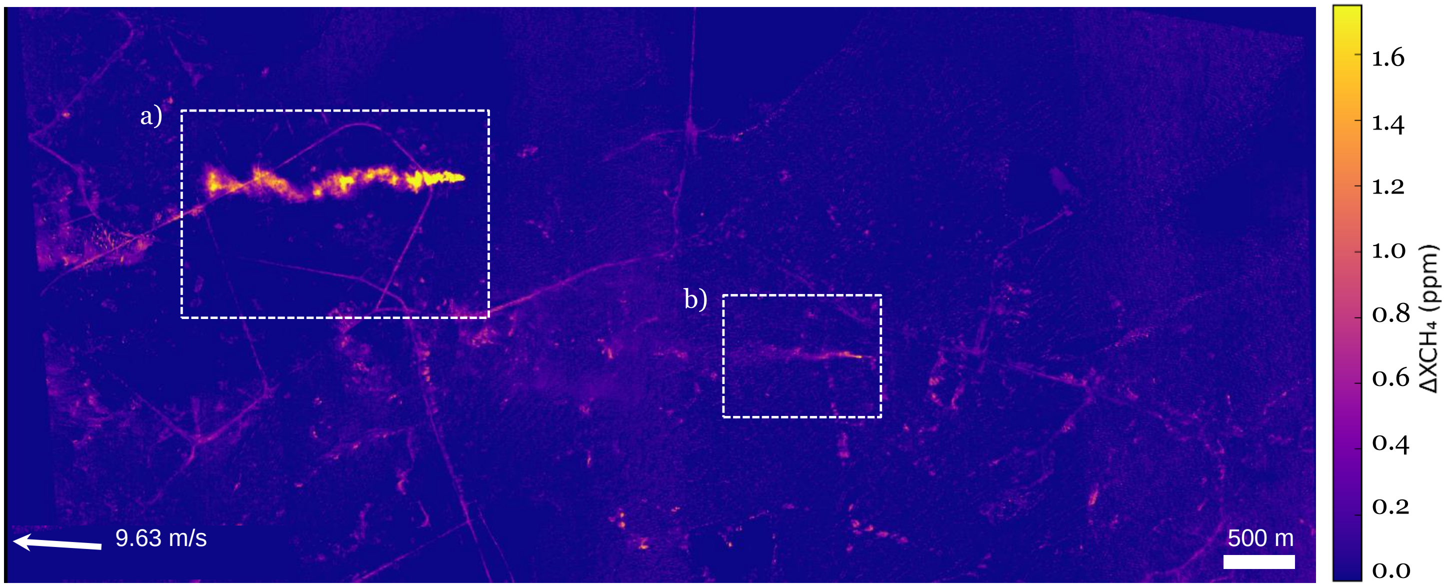

Real case studies of methane detection

√ **The area with the largest number of emitters** corresponds to the **Goturdepe O&G field** in North Turkmenistan.

A total of 16 different plumes are detected throughout this basin, one of the oldest oil piping systems.

Eastern image on 10th April 2021:

Dark color of the soil in the images indicate that oil burning works are taking place in the area.

- The biggest plume a) emerges from a thin pipeline coming out of the oil power plant adjoining.
- The origin of the other plume b) is not so obvious, likely caused by leakage from the **piping system** of the area.

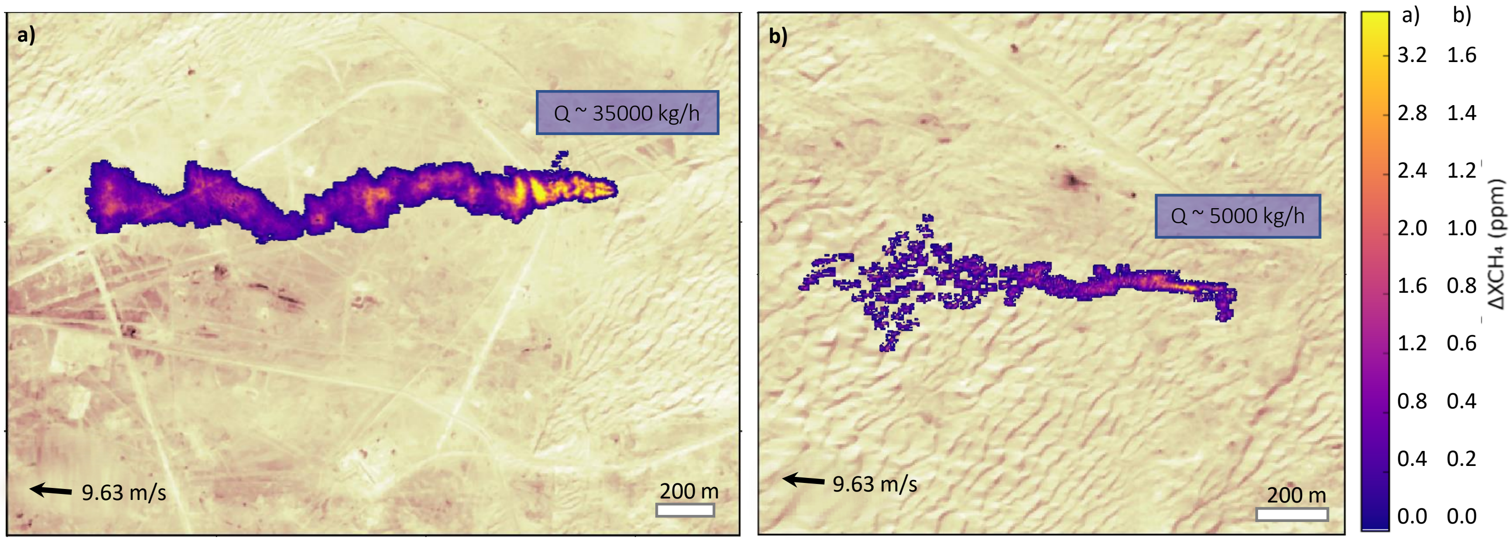

Real case studies of methane detection

Western image on 29th March 2021 → high number of small methane leakages that WV-3 has been able to reveal.

1. At a first glance, an apparent single plume northwest of the image & another towards the center.

1. However, by zooming in closer and considering the wind direction is possible to disentangle each of the underlying and independent emitting points, even unfolding those principal sources.

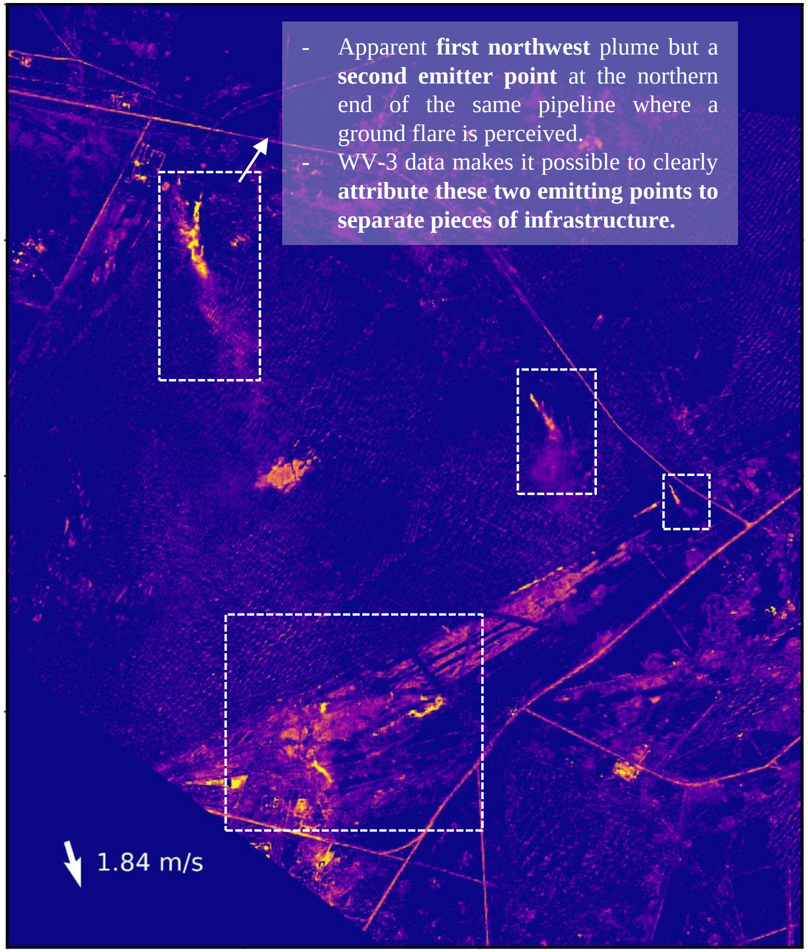

Real case studies of methane detection

Western image on 29th March 2021 → high number of small methane leakages that WV-3 has been able to reveal.

1. At a first glance, an apparent single plume northwest of the image & another towards the center.
2. However, by zooming in closer and considering the wind direction is possible to disentangle each of the underlying and independent emitting points, even unfolding those principal sources.

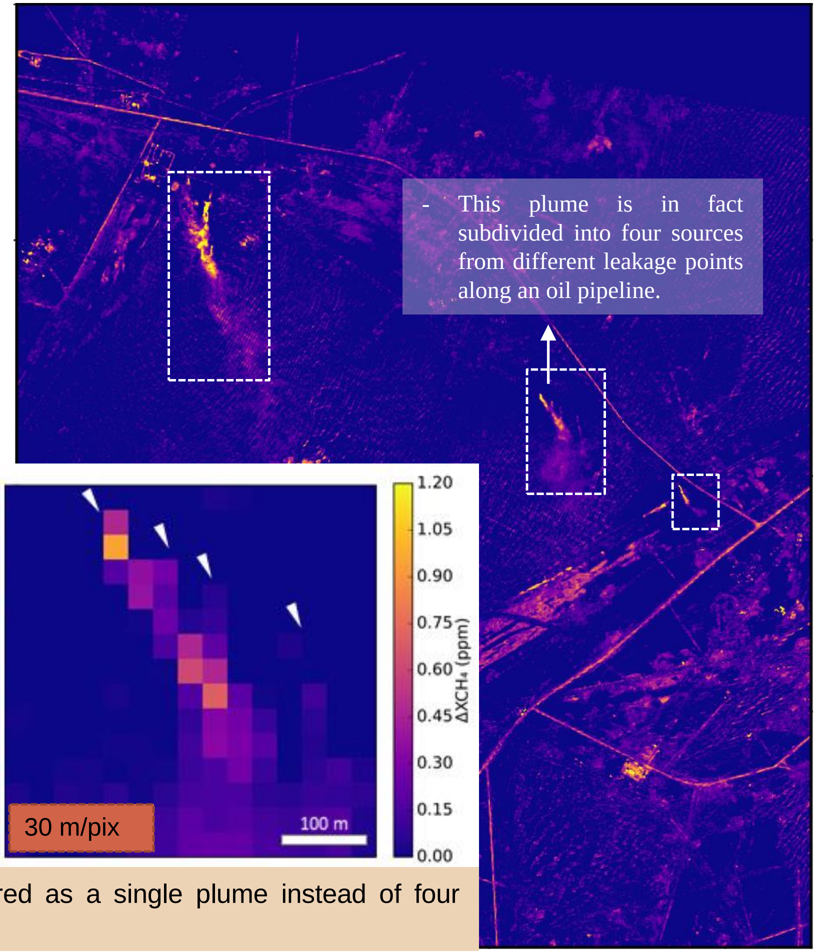

- This plume is in fact subdivided into four sources from different leakage points along an oil pipeline.

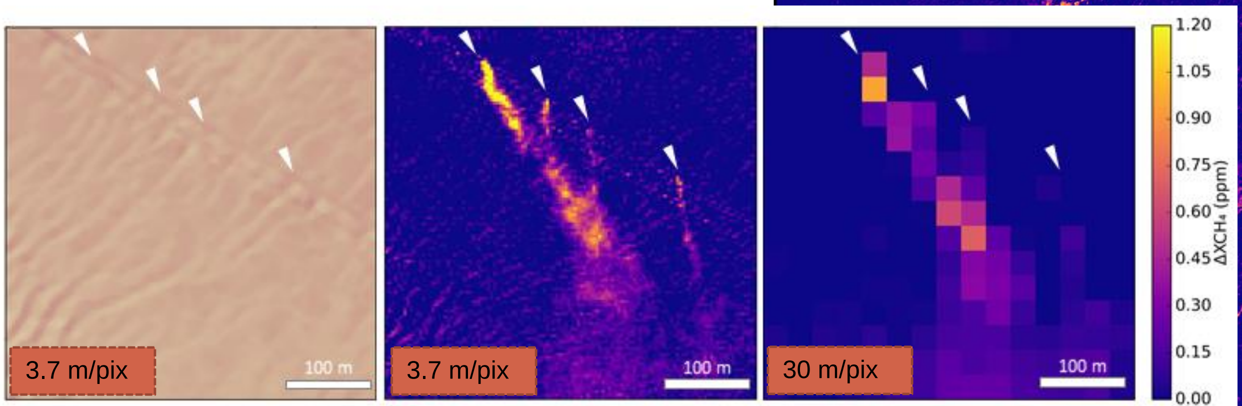

At 30 m/pix the ≠ point leakages are not identified, registered as a single plume instead of four independent sources.

Real case studies of methane detection

Western image on 29th March 2021 → high number of small methane leakages that WV-3 has been able to reveal.

1. At a first glance, an apparent single plume northwest of the image & another towards the center.

1. However, by zooming in closer and considering the wind direction is possible to disentangle each of the underlying and independent emitting points, even unfolding those principal sources.

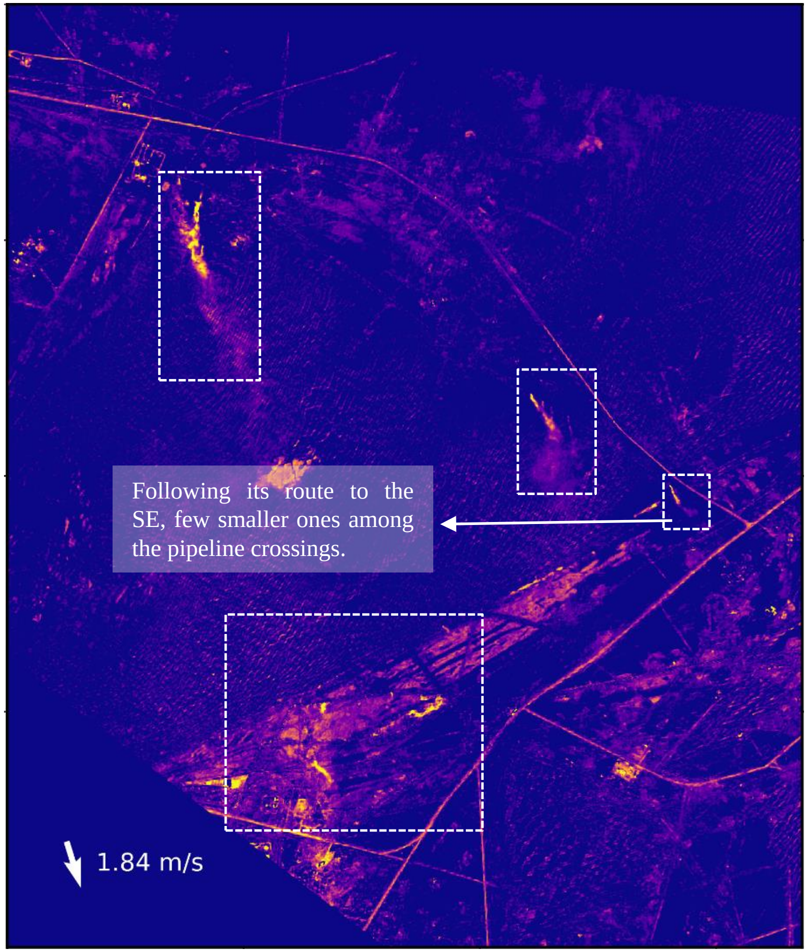

Real case studies of methane detection

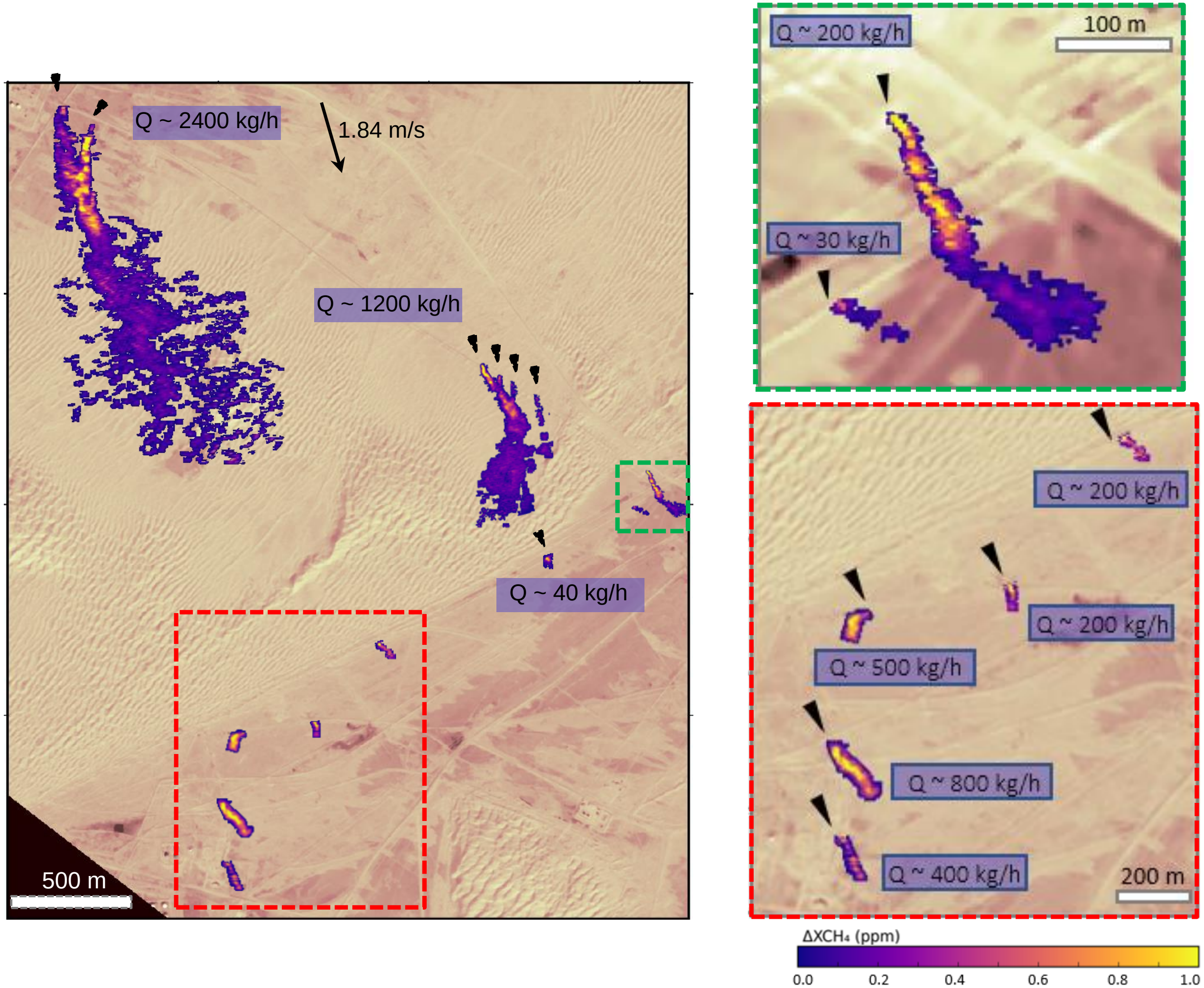

√ Some of these small leaks would go unnoticed by most satellites with lower spatial resolution and worse specifications for methane detection.

Real case studies of methane detection

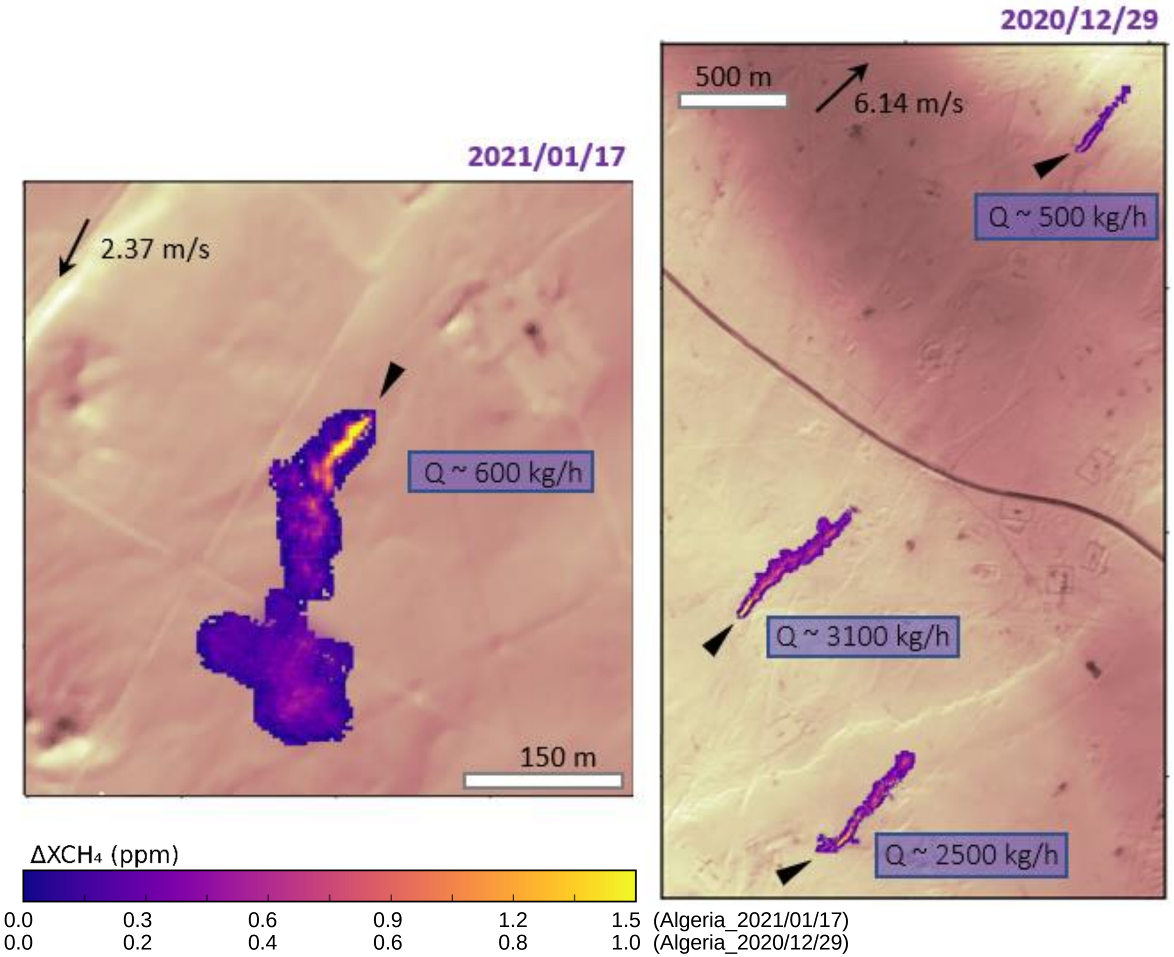

√ Algeria 29/12/2020:

- **Three elongated plumes** emerging **from different pipelines** perfectly aligned with wind direction, and with emission concentration values steadily decreasing due to the relatively **high wind speed** (6.14 m/s).
- Fast dispersion of the plume at about 500 m travel, blurring until the plume tail disappears.

√ On 17/01/2021:

- With **low wind speed** (2.37 m/s) the **high concentrations of the gas remain concentrated near the emitting point** defining a shorter plume.

Real case studies of methane detection

√ To further demonstrate the value of methane plume detection at 3.7 m pixel resolution:

Comparing ΔXCH_4 map obtained from the Algeria image on 29/12/2020 with this same result but upsampled to 30 m resolution:

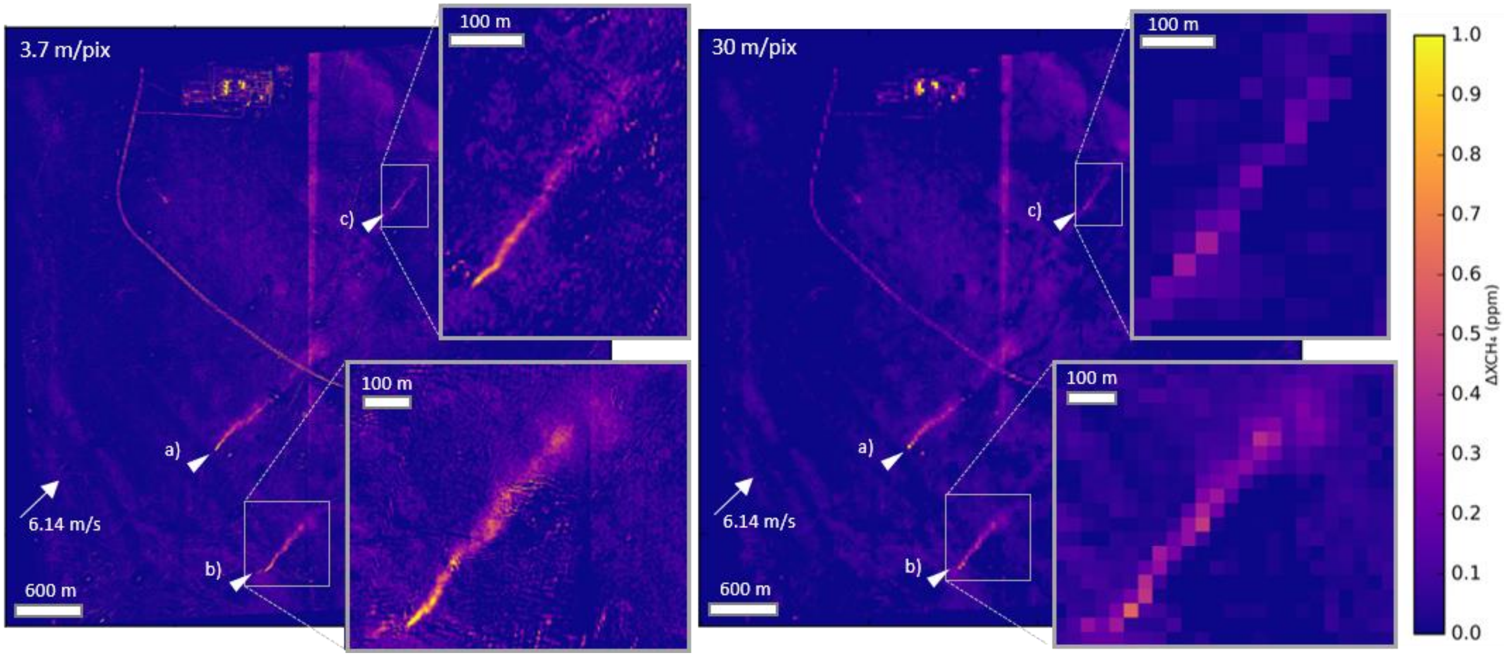

Coarser resolution → apart from **blurring the emitter point**, the **plumes** become more difficult to define, **especially the smaller one** which is **easily confused amid the background noise**.

RESULTS

Real case studies of methane detection

√ And some **emissions in the Shanxi coal mining** (west of the Zhangze reservoir) in China; image on 27/04/2021:

- Most **challenging site** for methane plume detection due to its **higher** spectral and spatial **heterogeneity** as simulations shown:

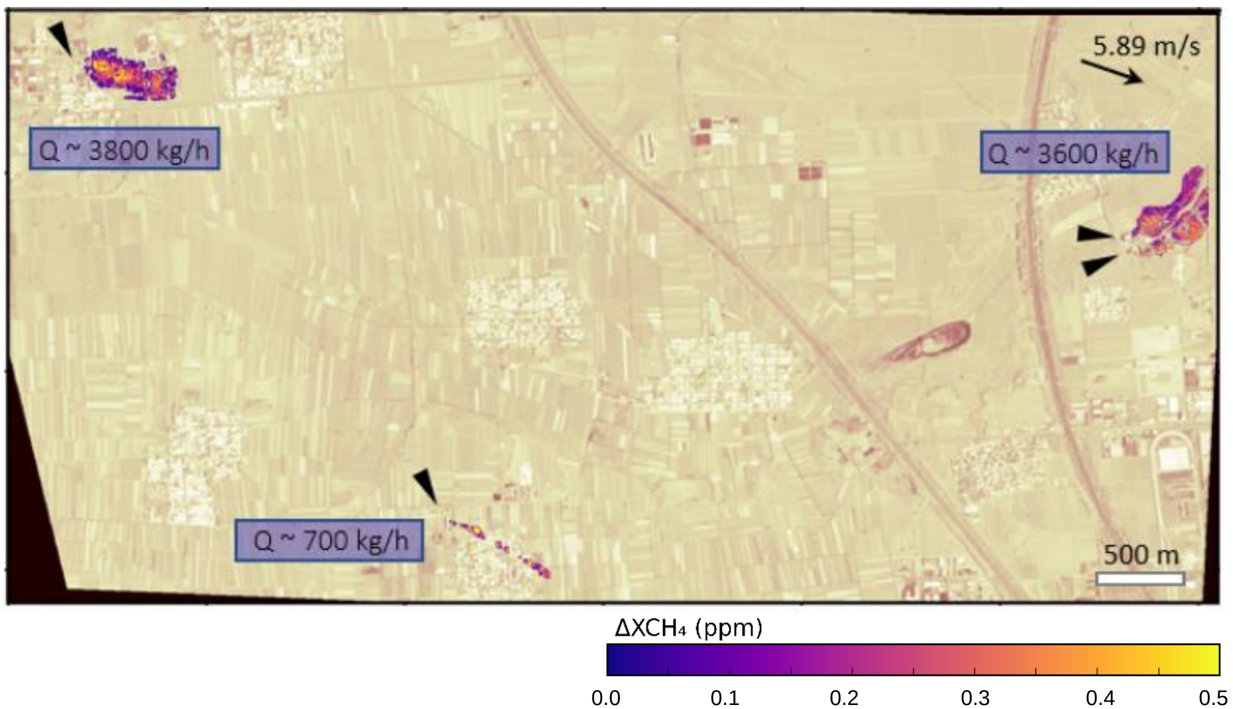

Table of contents

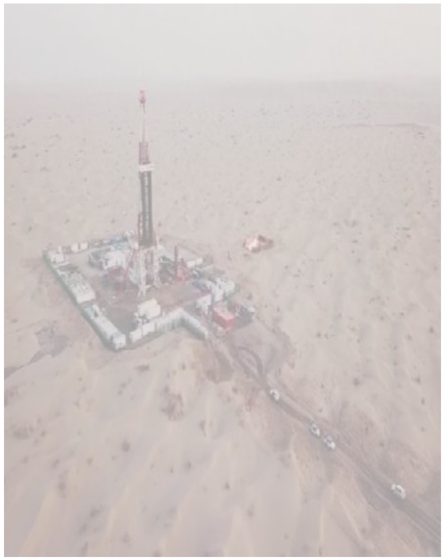

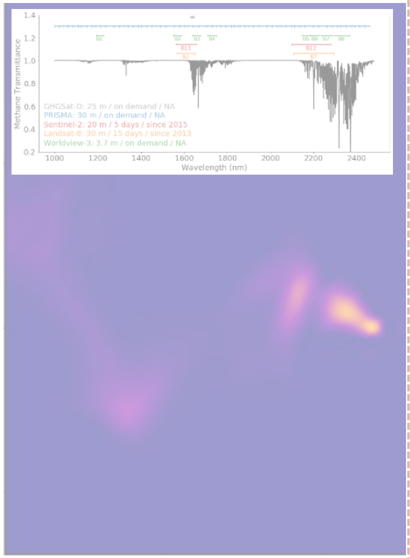

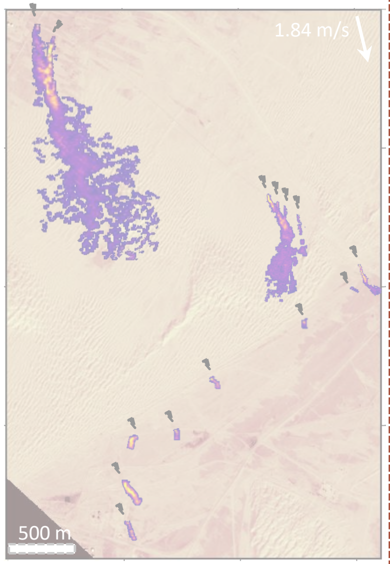

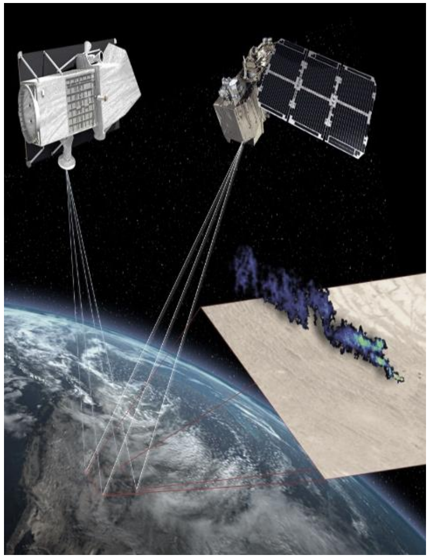

Conclusions

√ This **study reveals the** previously **undocumented capability of WV-3 for mapping methane** point source emissions at VH spatial resolution.

√ The **potential of WV-3** has been further tested under real-case studies with a positive **detection** of **26 independent point source emissions** covering different methane hotspot regions.

√ Under these real scenarios, we have proven the **usefulness of the unique spatial resolution** of the mission to even **pinpoint to very small leaks** (<100 kg/h) from oil pipelines in Turkmenistan that would be **missed by most satellites**
→ game-changing potential of **WV-3 to map industrial methane emissions** from space.

√ **The retrieval methodology is based on the MLR of 6 SWIR** bands **against B7** → weak sensitivity of the retrieval to the SRF of B7 and a negligible effect to the atmospheric WV column.

√ The **end-to-end sensitivity analysis** has helped to understand retrieval errors and detection limits → results over **homogeneous surfaces** with 21% IME loss ~10 Kg for a Q 1000 kg/h & 63% ~153 Kg for Q 1000 kg/h in highly **heterogeneous areas** such as the scene in China.

√ The Q uncertainties range 15-45% largely dominated by the uncertainty on the wind speed data.

Further research

√ **High spatial resolution** not only **helpful** to identify small sources of methane emissions but also **to detect outliers** (feature detection) → methane plume ~ soft edges whereas features (such as buildings and roads) ~ sharp edges.

√ **Despite the** promising results:

- Diminish the impact of the surface background and the plume parallax effects on the ΔXCH_4 maps → critical due to the higher variability of the surface at 3.7 m sampling and its orbit pointing capabilities that can result in large viewing zenith angles.
- A combination of the SWIR images with the VNIR data could improve both the regression and the identification of emission infrastructure.

√ The **ability to precisely locate and identify these emitting points** could **help steer the decision-making process** for repairing such pipeline leaks, delivering strong environmental and socioeconomic impacts → definition of a future CH_4 observing system as proposed by EU regulations.

References

Guanter, L., Irakulis-Loitxate, I., Gorroño, J., Sánchez-García, E., Cusworth, D.H., Cogliati, S., Colombo, R., 2021. Mapping methane point emissions with the PRISMA spaceborne imaging spectrometer. Remote Sens. Environ. https://doi.org/10.31223/X5VC9C

Irakulis-loitxate, I., Guanter, L., Liu, Y., Varon, D.J., Joannes, D., Zhang, Yuzhong, Thorpe, A.K., Duren, R.M., Lyon, D., Hmiel, B., Cusworth, D.H., Zhang, Yongguang, Segl, K., Gorroño, J., Sánchez-García, E., Sulprizio, M.P., Cao, K., Zhu, H., Liang, J., Li, X., Aben, I., Jacob, D.J., 2021a. Satellite-based Survey of Extreme Methane Emissions in the Permian Basin.

Irakulis-Loitxate, I., Guanter, L., Maasakkers, J.D., Zavala-Araiza, D., Aben, I., 2021b. Satellites unveil easily-fixable super-emissions in one of the world's largest methane hotspot regions [preprint] 1–32.

Lauvaux, T., Giron, C., Mazzolini, M., Duren, R., Cusworth, D., Shindell, D., Ciais, P., 2021. Global Assessment of Oil and Gas Methane Ultra-Emitters.

Varon, D.J., Jacob, D.J., Jervis, D., Mckeever, J., 2020. Quantifying Time-Averaged Methane Emissions from Individual Coal Mine Vents with GHGSat - D Satellite Observations. https://doi.org/10.1021/acs.est.0c01213.

Varon, D.J., Jacob, D.J., Mckeever, J., Jervis, D., Durak, B.O.A., Xia, Y., Huang, Y., 2018. Quantifying methane point sources from fine-scale satellite observations of atmospheric methane plumes 5673–5686.

Varon, D.J., Jervis, D., McKeever, J., Spence, I., Gains, D., Jacob, D.J., 2021. High-frequency monitoring of anomalous methane point sources with multispectral Sentinel-2 satellite observations. Atmos. Meas. Tech. 14, 2771–2785. https://doi.org/10.5194/amt-14-2771-2021.

Varon, D.J., McKeever, J., Jervis, D., Maasakkers, J.D., Pandey, S., Houweling, S., Aben, I., Scarpelli, T., Jacob, D.J., 2019. Satellite discovery of anomalously large methane point sources from oil/gas production. Geophys. Res. Lett. 2019GL083798. https://doi.org/10.1029/2019GL083798.

Thank you for your attention!!

Contact us:
https://hiresch4.upv.es/

There is one planet, one chance…